

Random-projection ensemble dimension reduction

Wenxing Zhou and Timothy I. Cannings

*School of Mathematics and Maxwell Institute for Mathematical Sciences
University of Edinburgh*

Abstract

We introduce a new framework for dimension reduction in the context of high-dimensional regression. Our proposal is to aggregate an ensemble of random projections, which have been carefully chosen based on the empirical regression performance after being applied to the covariates. More precisely, we consider disjoint groups of independent random projections, apply a base regression method after each projection, and retain the projection in each group based on the empirical performance. We aggregate the selected projections by taking the singular value decomposition of their empirical average and then output the leading order singular vectors. A particularly appealing aspect of our approach is that the singular values provide a measure of the relative importance of the corresponding projection directions, which can be used to select the final projection dimension. We investigate in detail (and provide default recommendations for) various aspects of our general framework, including the projection distribution and the base regression method, as well as the number of random projections used. Additionally, we investigate the possibility of further reducing the dimension by applying our algorithm twice in cases where projection dimension recommended in the initial application is too large. Our theoretical results show that the error of our algorithm stabilises as the number of groups of projections increases. We demonstrate the excellent empirical performance of our proposal in a large numerical study using simulated and real data.

Keywords: High-dimensional, mean central subspace, random projection, singular value decomposition, sufficient dimension reduction.

1 Introduction

In regression, we seek to understand the relationship between a p -dimensional vector of predictors X and a real-valued response variable Y , based on a sample of n observations from the target population. In many modern datasets, the number of predictors p is often large, and can even exceed the number of observations n in the dataset. This ‘large p , small n ’ setting frequently arises across various applications, for example, in biomedicine, -omics data often consists of measurements on many thousands of genes (Horvath, 2013; Bell et al.,

2019). In these high-dimensional problems, many conventional regression methods suffer from the *curse of dimensionality* and may even become intractable. For instance, ordinary least squares is not applicable when $p > n$ because the solution involves the inverse of a singular sample covariance matrix. Moreover nonparametric methods, which are often based on smoothness assumptions, hinge on having a sufficient quantity of data around the points of interest for prediction. As a result, the number of observations n required for such methods scales exponentially as the number of predictors p increases (see, for example, [Wainwright, 2019](#), Chapter 1.2).

There are two fundamental strategies that attempt to address this curse of dimensionality. The first approach balances model fit and model complexity via regularisation. In particular, in linear regression problems, the extremely popular and widely studied *ridge* ([Hoerl and Kennard, 1970](#)), *lasso* ([Tibshirani, 1996](#)) and *elastic net* ([Zou and Hastie, 2005](#)) algorithms provide elegant solutions. The latter two approaches operate on the assumption of *sparsity* that only a few variables have explanatory effects on the response, enabling these algorithms to identify a suitable subset of the predictors while simultaneously performing prediction. This is particularly appealing due to the simple interpretation that can be derived from the output. However, if the relationship between the predictors and the response is nonlinear, or if many of the variables are important, then these approaches may fail. The second strategy is to directly target a low-dimensional representation of the predictors, while still retaining the essential information on the relationship between X and Y . In particular, one general approach, called *sufficient dimension reduction* (SDR) ([Cook and Weisberg, 1991](#); [Cook et al., 2007](#); [Adragni and Cook, 2009](#)), aims to find a function $f : \mathbb{R}^p \rightarrow \mathbb{R}^d$, for some $d < p$, such that X and Y are independent given $f(X)$. A closely related problem focuses on the so-called *central mean subspace* ([Cook and Li, 2002](#)), where the conditional mean of Y given X can be written in terms of $f(X)$. By restricting f to be linear, these approaches are able to offer interpretable results, since the components in the low-dimensional representation may be more easily understood than those in the original p -dimensional vector.

In this paper, we propose a new method called *random projection ensemble dimension reduction* (see [Algorithm 1](#)). The main idea is to apply many low-dimensional random projections to the data, fit a base regression model after each projection and choose *good* projections according their empirical performance. We then aggregate the chosen projections using singular value decomposition. [Figure 1](#) below presents an example of our random projection-based method in a toy regression problem. We see that a randomly chosen 2-dimensional projection retains very little of the relationship between X and Y , but a projection carefully selected from a group of $L = 200$ random ones yields more promising results. Ultimately, by repeating this process and aggregating the chosen projections, we are able to retain a large amount of the structure observed after applying the oracle projection.

Our proposed framework is highly flexible and allows for user-specified choices of the random projection distribution and base regression method depending on the problem at hand. We investigate in detail the choice of several aspects of our algorithm. This includes, in [Section 3.1](#), the choice of the random projection distribution, where we find that simply

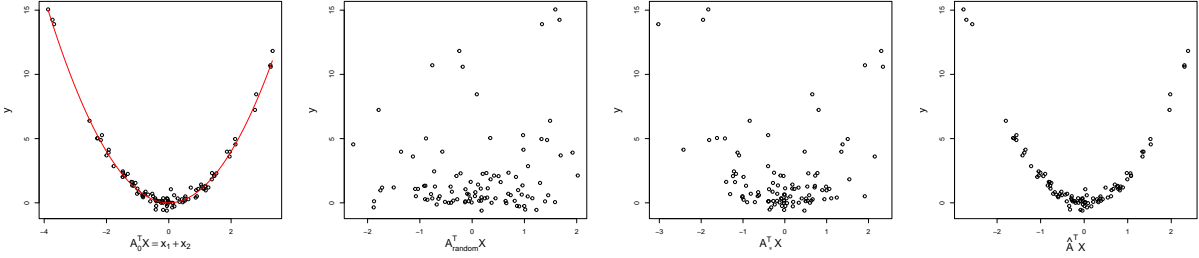


Figure 1: Dimension reduction example with $n = 100$ observations in $p = 20$ dimensions. The true model is $Y = A_0^T X + 0.3\epsilon$, with $A_0 = (1/\sqrt{2}, 1/\sqrt{2}, 0, \dots, 0)^T \in \mathbb{R}^{20}$, $X \sim N_{20}(0, I)$ and $\epsilon \sim N(0, 1)$. Far left: Y plotted against the oracle projection $x_1 + x_2$, the red line shows the true regression function. Middle left: Y plotted against a random projection. Middle right: Y plotted against the best projection among a group of 200 random projections. Far right: Y plotted against the projection estimated by our proposed method (with $L = 200$ groups).

using Gaussian projections is not always the best approach, particularly when the rows of the true projection matrix are sparse. In such cases projections with rescaled Cauchy entries perform better. Based on our results, we recommend using an equal mixture of rescaled Gaussian and Cauchy projections, which are competitive in both the sparse and dense regimes. We also compare the performance of our algorithm with different base regression methods. As demonstrated in Section 3.2, simple parametric (linear and quadratic) models perform very well when they are correctly specified in the low-dimensional space, but potentially suffer prohibitively if they are misspecified. In this case, we recommend using more flexible nonparametric models, with multivariate adaptive regression splines (MARS) (Friedman, 1991) emerging as a particularly effective choice. Our theoretical results (Theorem 1) show that the error of our approach converges at a rate no slower than $L^{-1/2}$, where L is the number of groups of projections considered. This rate is observed in our empirical investigations, which also consider the choices of the number of projections in each group and the dimension of the random projections; see Section 3.3.

One of the key features of our algorithm is that the output from the singular value decomposition step, namely the diagonal matrix of singular values, provides a measure of relative importance of the corresponding singular vectors. These values can therefore be used to determine a suitable projection dimension if this is not known in advance. We propose in Algorithm 2 in Section 3.4 to choose the projection dimension by comparing the singular values with those obtained when the group size is one (i.e. when no selection of *good* random projections is performed).

In Section 4, we demonstrate that the performance of our algorithm can perhaps be further improved by applying it a second time on the projected data from the initial application. In some cases, the combination of Algorithms 1 and 2 performs well in terms of the false negative rate (i.e. they output a projection that contains a majority of the true signals, but may also include additional ‘noise’ directions that are not needed). One way of viewing this is that the initial application acts more like a screening step, removing some

of the noise directions and preserving the signal directions. A second application of our algorithm (see Algorithm 3) applied to the projected data, can then refine the projection by combining signals and removing irrelevant directions.

We demonstrate the performance of our algorithms through a large numerical study using simulated data in Section 5, and real data in Section 6. Our proposal is very competitive in terms of empirical performance across a wide range of different settings. Code to implement our algorithms in R is available via GitHub¹.

Work on sufficient dimension reduction dates back to the idea of *inverse regression*, where in contrast to regressing Y on X , we target the expectation of X given Y . The earliest work in this area is *sliced inverse regression* (SIR) (Li, 1991), which uses ‘slices’ of the response Y to estimate $\text{Cov}(X | Y)$, then the eigenvectors of this estimate are used as the basis of the dimension reduction space. This idea led to a long line of work on inverse regression, including, among many others, *sliced average variance estimation* (SAVE) (Cook and Weisberg, 1991), *principal Hessian directions* (PHD) (Li, 1992), *sparse SIR* (Li and Nachtsheim, 2006) and *directional regression* (DR) (Li and Wang, 2007). In another line of work, the nonparametric *minimum average variance estimation* (MAVE) (Xia et al., 2002) algorithm estimates the dimension reduction space by constructing a minimization problem that quantifies how the dimension reduction model fits the observations. Ma and Zhu (2012) propose a semiparametric based approach, which take advantage of influence functions (Hampel, 1968) to construct a new kind of estimator. An excellent overview of these methods, as well as many other early works, is provided in the review article by Ma and Zhu (2013). More recent proposals include, *gradient based kernel dimension reduction* (gKDR) (Fukumizu and Leng, 2014), *deep SDR* (Banijamali et al., 2018; Kapla et al., 2022), *conditional variance estimator* (CVE) (Fertl and Bura, 2022) and *dimension reduction and MARS* (drMARS) (Liu et al., 2023); see also the recent review article by Ghojogh et al. (2021).

Random projections offer a natural approach to dimension reduction, and the celebrated Johnson–Lindenstrauss Lemma (Johnson and Lindenstrauss, 1984; Dasgupta and Gupta, 2003) shows that applying a random projection to the data may approximately preserve the pairwise distances between the observations. However, as illustrated in Figure 1, naively applying a single random projection typically fails. Our proposal is motivated by the work of Cannings and Samworth (2017), who propose a random projection ensemble method for binary classification based on aggregating the results of applying a base classifier to many carefully selected random projections of the data. Related ideas have been used more recently in the context of sparse principal component analysis (Gataric et al., 2020), sparse sliced inverse regression (Zhang et al., 2023) and semi-supervised learning (Wang et al., 2024). Other works on (unsupervised) dimension reduction using random projection techniques include Bingham and Mannila (2001) and Reeve et al. (2024). Random projection based techniques have been used in a wide range of other statistical applications, including precision matrix estimation (Marzetta et al., 2011), two-sample testing (Lopes et al., 2011), clustering (Fern and Brodley, 2003; Anderlucci et al., 2022), high-dimensional

¹<https://github.com/Wenxing99/RPEDR>

regression (Thanei et al., 2017; Slawski, 2018; Dobriban and Liu, 2019; Ahfock et al., 2021) and differentially private learning (Huang et al., 2024). See also the survey papers by Xie et al. (2017) and Cannings (2021).

The remainder of our paper is as follows: in Section 2 we formally introduce our statistical setting and present our main algorithm, Section 3 focuses on various practical considerations and provides recommendations on how to choose the inputs to our algorithm. In Section 4 we investigate the potential improvement gained by a second application of our main algorithm. The results of our numerical experiments with simulated and real data are presented in Sections 5 and 6, respectively. We conclude our paper with a discussion in Section 7. The Appendix contains the proofs of our theoretical results (Section A), as well as the full results of our large simulation study (Section B).

2 Statistical setting and methodology

Let P denote a distribution on $\mathbb{R}^p \times \mathbb{R}$ and suppose that the covariate-response pair $(X, Y) \sim P$. Let $\eta(x) := \mathbb{E}(Y \mid X = x)$ be the regression function. We seek to find a dimension $d \in \{1, \dots, p-1\}$ and a corresponding projection matrix $A \in \mathcal{A}_{p \times d} := \{A \in \mathbb{R}^{p \times d} : A^T A = I_{d \times d}\}$ for which there exists a function $g : \mathbb{R}^d \rightarrow \mathbb{R}$ satisfying

$$\eta(x) = g(A^T x). \tag{1}$$

Here A^T maps X onto a d -dimensional subspace, and when $d < p$ the lower-dimensional representation $A^T X$ contains all the information available in X about the conditional mean of Y given X .

Equation (1) is of course satisfied by taking $d = p$, $A = I_{p \times p}$ (the p -dimensional identity matrix) and $g = \eta$. The main interest, however, is in finding a solution to (1) for a minimal choice of d , which we will denote by d_0 . The corresponding projection matrix and link function will be denoted by A_0 and g_0 , respectively. While d_0 is unique, the associated A_0 is not. Indeed, if $A_0 \in \mathcal{A}_{p \times d_0}$ and g_0 satisfy (1), then so do $A_1 = A_0 B$ and $g_1(\cdot) = g_0(B \cdot)$, for any $B \in \mathcal{A}_{d_0 \times d_0}$.

Since A_0 is not uniquely identifiable, our focus is on the space spanned by the columns of A_0 . For a projection matrix $A \in \mathcal{A}_{p \times d}$, we write $\mathcal{S}(A) = \text{span}(A)$ for the d -dimensional subspace spanned by the columns of A . If A satisfies (1), then $\mathcal{S}(A)$ is called a *mean dimension reduction subspace* (Cook and Li, 2002). The space spanned by the columns of the d_0 -dimensional projection A_0 , $\mathcal{S}(A_0)$, is called the *central mean dimension reduction subspace*, or simply *central mean subspace (CMS)*.

For the purposes of this paper, we assume the existence and uniqueness of the CMS. This assumption allows us to focus on our main goal of estimating the space $\mathcal{S}(A_0)$ based on a dataset of n independent and identically distributed pairs $(X_1, Y_1), \dots, (X_n, Y_n) \sim P$. Our estimate in this problem will be the space spanned by the columns of a projection $\hat{A}_0 \in \mathcal{A}_{p \times \hat{d}_0}$ for some $\hat{d}_0 \in [p]$, say, where \hat{d}_0 and \hat{A}_0 are (possibly randomised) functions of the data $\mathcal{D} = \{(X_1, Y_1), \dots, (X_n, Y_n)\}$. There are many ways of measuring the distance between

the spaces $\mathcal{S}(\hat{A}_0)$ and $\mathcal{S}(A_0)$. We will primarily focus on the measure $d_F(\mathcal{S}(\hat{A}_0), \mathcal{S}(A_0))$, where

$$d_F^2(\mathcal{S}(\hat{A}_0), \mathcal{S}(A_0)) := \frac{1}{2} \|\hat{A}_0 \hat{A}_0^T - A_0 A_0^T\|_F^2. \quad (2)$$

The scaling in (2) ensures that, if $d_0 = \hat{d}_0$, then the measure d_F is equivalent to the sin-theta distance (Davis and Kahan, 1970; Yu et al., 2015).

2.1 The random projection ensemble dimension reduction algorithm

In this section, we formally introduce our new procedure for dimension reduction, which is presented in Algorithm 1 below. First, we outline some of the notation used, starting with the notion of a base regression method. Given a data set of n_1 covariate-response pairs $((z_1, y_1), \dots, (z_{n_1}, y_{n_1})) \in (\mathbb{R}^d \times \mathbb{R})^{n_1}$, a d -dimensional data-dependent regression method is a measurable function $\hat{g} : \mathbb{R}^d \times (\mathbb{R}^d \times \mathbb{R})^{n_1} \rightarrow \mathbb{R}$. The function \hat{g} uses the data $(z_1, y_1), \dots, (z_{n_1}, y_{n_1})$ to estimate a regression function $g : \mathbb{R}^d \rightarrow \mathbb{R}$. We write \mathcal{G}_{d, n_1} for the set of all such regression methods. In Algorithm 1, z_1, \dots, z_{n_1} are different (randomly chosen) projections of a subset of the p -dimensional covariate observations x_1, \dots, x_n .

Our algorithm also takes as inputs a projection dimension $d \in [p]$ alongside a corresponding projection distribution Q on $\mathcal{Q}_{p \times d} := \{A \in \mathbb{R}^{p \times d} : \text{diag}(A^T A) = (1, \dots, 1)^T\}$, a number of groups of projections $L \in \mathbb{N}$, a group size $M \in \mathbb{N}$ and a subsample size $n_1 \in [n]$, as well as a base regression method $\hat{g} \in \mathcal{G}_{d, n_1}$. A full investigation, alongside recommendations of how to choose these inputs in practice is given in Section 3.

Algorithm 1: Random projection ensemble dimension reduction

- 1 **Input:** Data $((x_1, y_1), \dots, (x_n, y_n)) \in (\mathbb{R}^p \times \mathbb{R})^n$, projection dimension $d \in [p]$, projection distribution Q on $\mathcal{Q}_{p \times d}$, number of groups L , group size M , sample-split size $n_1 \in [n - 1]$, base regression method $\hat{g} \in \mathcal{G}_{d, n_1}$.
 - 2 Let $\mathbf{P}_{1,1}, \dots, \mathbf{P}_{L,M} \stackrel{\text{i.i.d.}}{\sim} Q$.
 - 3 **for** $\ell \in [L]$ **do**
 - 4 Let \mathcal{N}_1 be a random sample of size n_1 chosen without replacement from $\{1, \dots, n\}$.
 - 5 **for** $m \in [M]$ **do**
 - 6 for $i \in \mathcal{N}_1^c$, let $\hat{h}_{\ell, m}(x_i) = \hat{g}(\mathbf{P}_{\ell, m}^T x_i; (\mathbf{P}_{\ell, m}^T x_j, y_j)_{j \in \mathcal{N}_1})$.
 - 7 let $\hat{R}_{\ell, m} = \sum_{i \in \mathcal{N}_1^c} \{y_i - \hat{h}_{\ell, m}(x_i)\}^2$.
 - 8 Choose the projection that minimizes the mean squared error within the group,
 $\mathbf{P}_{\ell, *} := \text{sargmin}_{m \in [M]} \hat{R}_{\ell, m}$
 - 9 Set $\hat{\Pi} := \frac{1}{L} \sum_{\ell=1}^L \mathbf{P}_{\ell, *} \mathbf{P}_{\ell, *}^T$
 - 10 Calculate the singular value decomposition of $\hat{\Pi} = U D U^T$
 - 11 **Output:** The matrix $U \in \mathbb{R}^{p \times p}$ and $\text{diag}(D) \in \mathbb{R}^p$.
-

Algorithm 1 starts by generating $L \cdot M$ random projection matrices $\mathbf{P}_{\ell,m} \in \mathbb{R}^{p \times d}$, where each is sampled from the specified distribution Q . These projections are partitioned into L disjoint groups of size M . For each projection $\mathbf{P}_{\ell,m}$, we apply it to the covariates and fit the base regression model \hat{g} using a subsample of the projected data. The performance of each projection is measured by the mean squared error on the complement of the training subsample and within each group, we retain the projection with the best performance. These selected projections, denoted $\mathbf{P}_{\ell,*}$, are then aggregated by taking the average of their outer products to give $\hat{\Pi}$. Finally, the algorithm outputs the $p \times p$ orthonormal matrix $U = (U_1, \dots, U_p)$ alongside the vector $\text{diag}(D)$, provided by the singular value decomposition of $\hat{\Pi}$.

The idea is that the columns of U contain the estimated dimension reduction directions, with the singular values D providing information about the relative importance of each direction. If the desired projection dimension \hat{d}_0 is predetermined, then we retain the first \hat{d}_0 columns and set $\hat{A}_0 = (U_1, \dots, U_{\hat{d}_0})$ as our estimate of A_0 . On the other hand, if \hat{d}_0 is not determined in advance, then the singular values provide a useful guide. In some cases, there may be a clear candidate choice of \hat{d}_0 , but when an appropriate choice is less obvious, we propose to choose \hat{d}_0 by comparing the output of Algorithm 1 with the corresponding output obtained when $M = 1$, i.e. compared with random matrices without selection (see Algorithm 2 in Section 3.4).

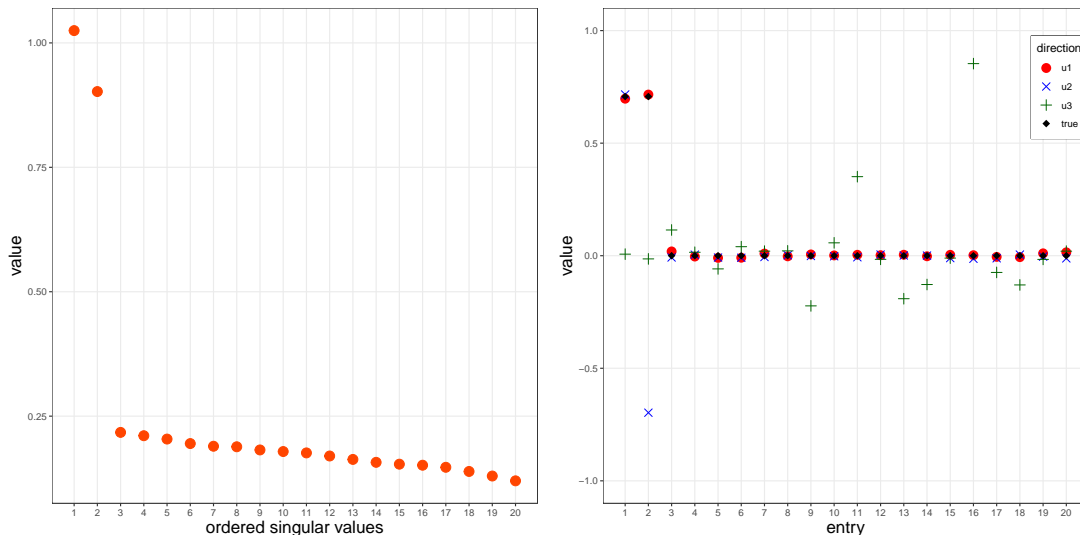


Figure 2: An example of some of the output from Algorithm 1 applied to the data used in Figure 1 with $p = 20$ and $n = 100$. Here we take $d = 5$, $L = 200$, $M = 200$, $n_1 = 66$, the random projections Q are taken to have independent standard Cauchy random variables, and \hat{g} the quadratic least-squares regressor. We present the entries of the diagonal matrix D (left plot), alongside the entries of the first (red filled circles), second (blue \times) and third (green $+$) columns of U (right plot). We also include the entries of the true dimension reduction direction (black filled diamonds).

To demonstrate how our approach works, we applied Algorithm 1 to the data used

in Figure 1. In Figure 2 we observe that the first two entries of D are relatively large, suggesting that the singular vectors U_1 and U_2 contain a large proportion of the signal. In this case, the true sufficient dimension reduction direction A_0 is one-dimensional and nearly all of the signal is found in the first singular vector, with $|U_1^T A_0| = 0.996$. The second singular vector here contains a small amount of the signal with $|U_2^T A_0| = 0.048$. The remaining entries of D are relatively small, suggesting that U_3, \dots, U_p can be discarded (indeed $\max_{j=3, \dots, p} |U_j^T A_0| < 0.01$).

3 Practical considerations

3.1 Random projection generating distribution

In this section, we investigate the effect of the random projection distribution in Algorithm 1. For brevity, we focus on two distributions:

1. *Gaussian rows*: Let Q_N denote the distribution $\mathcal{Q}_{p \times 1}$ formed by first generating p independent standard Gaussian random variables and then normalising the row to have unit norm. In other words, we say $\mathbf{Q} \sim Q_N$ if $\mathbf{Q} \stackrel{d}{=} Z/\|Z\|$, where $Z \sim N_p(0, I)$.
2. *Cauchy rows*: We write $\mathbf{Q} \sim Q_C$ if $\mathbf{Q} \stackrel{d}{=} W/\|W\|$, where $W = (W_1, \dots, W_p)$ and $W_1, \dots, W_p \stackrel{\text{i.i.d.}}{\sim} \text{Cauchy}(0, 1)$.

Projections with independent Gaussian entries are widely used in the literature and have desirable rotational invariance properties (see, for example, [Vershynin, 2018](#), Proposition 3.3.2). On the other hand, several works have explored the use of Cauchy random projections in various contexts, offering distinct advantages for certain applications. For example, [Li et al. \(2007\)](#) extended the Johnson-Lindenstrauss Lemma to the l_1 -norm using Cauchy random projections, while [Ramirez et al. \(2012\)](#) used them for sparse signal reconstruction.

We conduct a numerical experiment using three different versions of the following model:

- Model 1: Let $X \sim N_p(0, I)$ and $Y = 2(A_0^T X)^2 + \epsilon$, where $\epsilon \sim N(0, 1/4)$ and $A_0^T = \frac{1}{\sqrt{q}}(\mathbf{1}_q, \mathbf{0}_{p-q})$, for $q \in [p]$. Here $\mathbf{1}_q$ and $\mathbf{0}_{p-q}$ denote a q -dimensional vector of ones and a $(p - q)$ -dimensional vector of zeros, respectively.

We set $p = 20$ and vary q to simulate different sparsity levels, with $q = 2$ (Model 1a), $q = 10$ (Model 1b) and $q = 20$ (Model 1c). We consider three different projection distributions, namely $Q_N^{\otimes d}$ (Gaussian), $Q_C^{\otimes d}$ (Cauchy) and $\frac{1}{2}Q_N^{\otimes d} + \frac{1}{2}Q_C^{\otimes d}$ (mixture). The idea is to show the effect of the choice of random projection distribution for the different levels of sparsity. The experiment is designed in such a way that the signal strength is the same in each setting. The other inputs to Algorithm 1 are the same in each case. Indeed, in all the experiments in this subsection, we set $n = 200$, and the inputs to Algorithm 1 are $d = 5$, $L = 200$, $M = 200$, $n_1 = \lceil 2n/3 \rceil$, the base method \hat{g} is taken to be the global quadratic least squares estimator (see equation (3) for a formal definition).

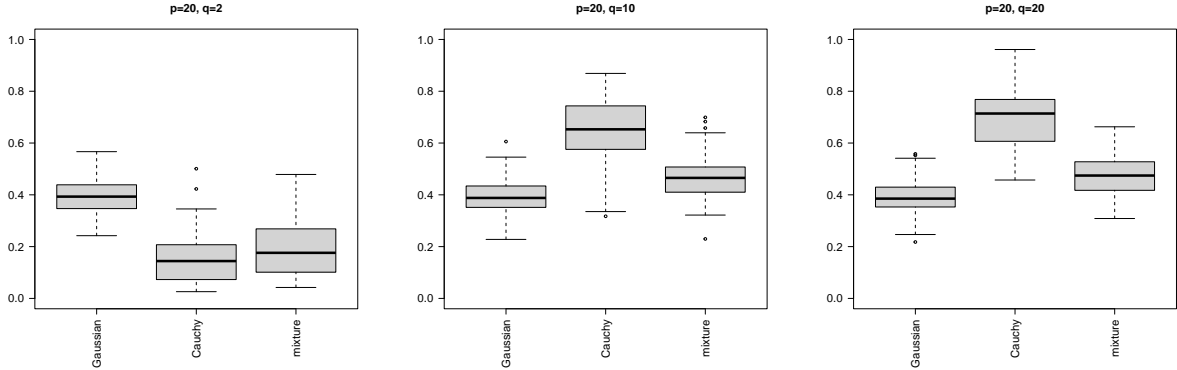


Figure 3: Boxplots of the sin-theta distance (see (2)) between U_1 from the output of Algorithm 1 and the true direction $A_0 = (\mathbf{1}_q, \mathbf{0}_{p-q})$ over 100 repeats of the simulation. We present the results for three different instances of Model 1, namely when $q = 2$ (left), $q = 10$ (middle) and $q = 20$ (right). We compare the results when the projection distribution Q is $Q_N^{\otimes d}$ (Gaussian), $Q_C^{\otimes d}$ (Cauchy), and $\frac{1}{2}Q_C^{\otimes d} + \frac{1}{2}Q_N^{\otimes d}$ (mixture).

Figure 3 shows that in sparse models Cauchy projections do indeed outperform Gaussian projections, but the heavy tailed Cauchy distribution is not well-suited to cases where there is no sparsity. As expected, due to the rotational invariance in the problem, Gaussian random projections exhibit the same performance regardless of the sparsity level. We see that using a fifty-fifty mixture of Gaussian and Cauchy projections in our algorithm leads to good performance regardless of the sparsity level, and if the practitioner has no knowledge of the sparsity level of A_0 , then we recommend using this mixture as the default option and indeed this strategy will be employed in all of the numerical experiments presented later in the paper.

3.2 Choice of base regression method

The choice of base regression method $\hat{g} \in \mathcal{G}_{d,n_1}$ used in Algorithm 1 depends on two primary factors. First, the method should be computationally efficient, as it will be applied $L \cdot M$ times to different randomly projected datasets. We delay our discussion of computational aspects of the problem to Section 3.5 and focus here on the second primary factor: the base regression method must capture at least some of the signal after a *good* projection has been applied. We will demonstrate that a global polynomial based method is often effective, even when the true signal is not exactly a polynomial. However, there are scenarios in which a more flexible nonparametric approach may be needed.

We investigate four options in detail. In each case, we describe how $\hat{g} \in \mathcal{G}_{d,m}$ is defined based on a dataset $(z_1, y_1), \dots, (z_m, y_m) \in (\mathbb{R}^d \times \mathbb{R})^m$ of size² $m > 1 + d(d+3)/2$ and a test

²this sample size requirement is mild and ensures that we can apply the global quadratic method below – if it is not satisfied, then either d should be reduced, or we may be limited to using the linear least squares method which only requires $m > d$.

point $z \in \mathbb{R}^d$.

1. Global linear least squares (LLS): $\hat{g}_{\text{GL}}(z) = \hat{\alpha} + \hat{\beta}^T z$, where

$$(\hat{\alpha}, \hat{\beta}) := \underset{(\alpha, \beta) \in \mathbb{R} \times \mathbb{R}^d}{\operatorname{argmin}} \left\{ \sum_{i=1}^m (y_i - \alpha - \beta^T z_i)^2 \right\}.$$

2. Global quadratic least squares (QLS): $\hat{g}_{\text{GQ}}(z) := \hat{a} + \hat{b}^T z + z^T \hat{C} z$, where

$$(\hat{a}, \hat{b}, \hat{C}) := \underset{(a, b, C) \in \mathbb{R} \times \mathbb{R}^d \times \mathbb{S}_{d \times d}}{\operatorname{argmin}} \left\{ \sum_{i=1}^m (y_i - a - b^T z_i - z_i^T C z_i)^2 \right\}, \quad (3)$$

and $\mathbb{S}_{d \times d}$ denotes the set of $d \times d$ symmetric matrices.

3. Nadaraya–Watson: Fix a kernel K and a bandwidth $h > 0$, then let

$$\hat{g}_{\text{NW}}(z) = \frac{\sum_{i=1}^m y_i K(h^{-1} \|z_i - z\|)}{\sum_{i=1}^m K(h^{-1} \|z_i - z\|)}.$$

In our experiments below, we take $K(t) = \frac{e^{-t^2/2}}{\sqrt{2\pi}}$ and $h = 0.1$.

4. Multivariate Adaptive Regression Splines (MARS): Let \hat{g}_{MARS} be Algorithms 2 and 3 of [Friedman \(1991\)](#), which fits piecewise linear models to the data and automatically selects interactions between variables. We use the implementation of this method from the R-package `earth` ([Milborrow, 2024](#)). The maximum degree of interaction is taken to be 3.

While many alternative base regression methods are available, we focus on these four methods for their balance of flexibility and computational feasibility.

To demonstrate how these different options perform in practice, we carry out a further set of experiments using three different models:

- Model 1a: as used in the previous subsection with $A_0 = (\mathbf{1}_2, \mathbf{0}_{p-2})^T$.
- Model 2: Let $X = (X_1, \dots, X_p)^T \sim \text{Unif}([-1, 1]^p)$ and $Y = 2 \sin(2\pi X_3) + \epsilon$ with $\epsilon \sim N(0, 1/4)$ independent of X .
- Model 3³: Let $X = (X_1, \dots, X_p)^T \sim N_p(0, I)$ and

$$Y = \frac{X_6}{1/2 + (X_7 + 3/2)^2} + \epsilon$$

with $\epsilon \sim N(0, 1/4)$ independent of X . Here $A_0 = (e_6, e_7)$ is 2-dimensional, where e_j denotes the j th canonical Euclidean basis vector in \mathbb{R}^p .

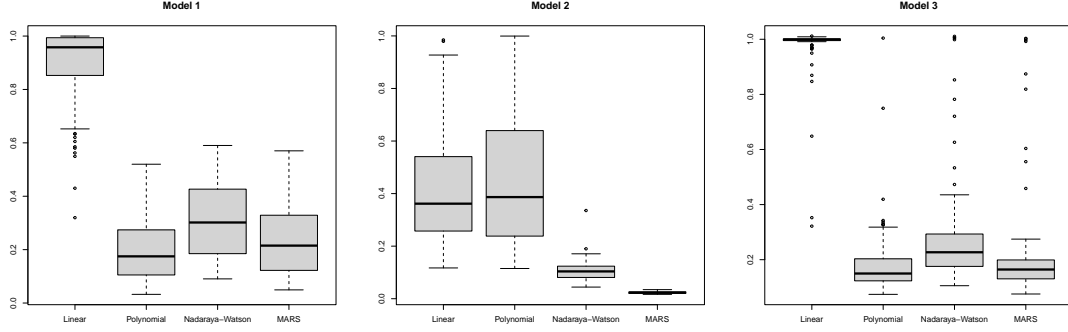


Figure 4: Boxplots of the sin-theta distance (see (2)) between $U_{1:d_0}$ from the output of Algorithm 1 and the true direction A_0 over 100 repeats of the simulation. We present the results for Model 1a (left), Model 2 (middle) and Model 3 (right), for $p = 20$ and $n = 200$. The base method is linear least squares, quadratic least squares, Nadaraya-Watson or the MARS algorithm.

In each case, we set $p = 20$ and $n = 200$ and apply Algorithm 1 with $d = 5$, $L = 200$, $M = 200$, $n_1 = \lceil 2n/3 \rceil$, and $Q = \frac{1}{2}Q_N^{\otimes d} + \frac{1}{2}Q_C^{\otimes d}$.

Figure 4 exhibits some interesting behaviour. In Model 1a, the linear regression base method is not effective because no linear signal exists in any d -dimensional projection of the data. For a similar reason, the linear and quadratic least squares methods do not perform well in Model 2. However, in Model 1a, the quadratic base method is very effective, as this model is correctly specified after applying the oracle projection A_0 . MARS also performs well here, although at a higher computational cost. For Model 2, the flexibility of the nonparametric methods is required to find the signal, and MARS outperforms the Nadarya-Watson base method. The results for Model 3 show that, even when the base model is incorrectly specified, good performance is still achieved. Here the true regression function after the oracle projection is not a polynomial. The linear base method is effective in finding the (approximately) linear signal in X_6 , but does not find any of the signal in X_7 . However, the signal is sufficiently well-approximated by a quadratic function that we are able to find a lot of the signal with a the quadratic base method. Here the slightly more computationally expensive MARS algorithm performs similarly to the quadratic least squares approach.

Based on results in this section, MARS is recommended as a suitable default base regression method. It performs well across all examples presented here, as well as in a broad range of settings in our large simulation study in Section 5.

3.3 Choice of L , M and d

Our Algorithm 1 combines the results of assessing the empirical performance of the base regression method in a total of $L \cdot M \cdot d$ projection directions. More precisely, we aggregate the results of L (d -dimensional) projections, where each projection is selected as the best

³Model 3 was used in the simulation studies in Li (1991); Xia et al. (2002); Liu et al. (2023).

out of a (disjoint) block of size M . In this section, we explore how varying these parameters affects performance. As we will show, the performance typically improves as L increases, in the sense that the sin-theta distance decreases at rate $L^{-1/2}$ (assuming the other quantities are kept fixed); see Theorem 1 and our numerical results in Figure 5. Overall, the results in this section lead to our recommendation of a default choice of $L = 200$. The effect of the parameters M and d is slightly less straightforward, and their choices are influenced by the ambient dimension p . Indeed, ultimately we recommend taking $M = 10p$ and $d = \lceil p^{1/2} \rceil$.

We first focus on the choice of L . Theorem 1 below compares the sin-theta distance between the first d_0 columns of U from the output of Algorithm 1 applied with L projections, with the corresponding output when considering an infinite simulation version of our algorithm which takes “ $L = \infty$ ”. More precisely, given data $\{(x_1, y_1), \dots, (x_n, y_n)\}$ (here considered to be fixed pairs in $\mathbb{R}^p \times \mathbb{R}$), $d \in [p]$, $Q \in \mathcal{Q}_{d \times p}$, $L \in \mathbb{N}$, $M \in \mathbb{N}$, $n_1 \in [n - 1]$ and $\hat{g} \in \mathcal{G}_{d, n_1}$, let $\hat{A}_0^L := \hat{A}_0 = (U_1, \dots, U_{d_0})$ denote the first d_0 columns of the output of Algorithm 1. Here we assume knowledge of the true d_0 and explicitly emphasise the dependence on L . Further define $\Pi^\infty := \mathbb{E}(\mathbf{P}_{\ell, *}, \mathbf{P}_{\ell, *}^T) \in \mathbb{S}_{p \times p}$ to be the expected value of $\hat{\Pi}$ in line 9 of Algorithm 1. Here the expected value is taken only over the randomness in the projections and in the sample-split in line 4 of the algorithm, but not the data. Let $\hat{A}_0^\infty := (U_1^\infty, \dots, U_{d_0}^\infty)$, where $U_1^\infty, \dots, U_p^\infty$ are the singular vectors of Π^∞ .

Theorem 1. *We have*

$$\mathbb{E}d_{\mathbb{F}}(\mathcal{S}(\hat{A}_0^L), \mathcal{S}(A_0)) \leq 2d_0^{1/2} \|\Pi^\infty - A_0 A_0^T\|_{\text{op}} + \frac{2d_0^{1/2} (2\pi)^{1/2} p}{L^{1/2}}.$$

The proof of Theorem 1 is given in Section A. The second term in the bound given by Theorem 1 suggests that the error of our algorithm decreases at a rate of $L^{-1/2}$ as L increases. Our numerical results below suggest that this is typically the case in practice. The first term in the bound does not depend on L , and can be seen as the infinite simulation error of our method. This term depends on the choice of M and d (as well as the base regression method and projection distribution) and would be small when, on average, the projections selected are close to A_0 . Since A_0 is unknown, determining a theoretically optimal choice of M and d seems intractable and we will instead provide recommendations based on the empirical experiments below – see Figure 6.

To further elucidate the effect of L in practice, we conduct a numerical experiment using versions of Models 1a, 2 and 3 from the previous subsection with $p = 20$ and $p = 100$; see Figure 5. We set $n = 200$, with the other inputs to Algorithm 1 being $d = 5$, $M = 10p$, $n_1 = \lceil 2n/3 \rceil$, $Q = \frac{1}{2}Q_{\mathbb{C}}^{\otimes d} + \frac{1}{2}Q_{\mathbb{N}}^{\otimes d}$ for the projection distribution, and \hat{g} being the MARS algorithm. The number of projections L varies from 10 to 1000.

The empirical results in Figure 5 confirm that in these examples, we can expect the performance of our algorithm to improve as L increases as indicated by Theorem 1. In the results for Model 1, we observe a larger variance across different repeats of the experiment – this is due in part to the fact that, in this example, our algorithm captures only part of the true signal in the leading order singular vector in U . As discussed later in Section 5, our method performs well here in the sense that nearly all of the signal is found in the first

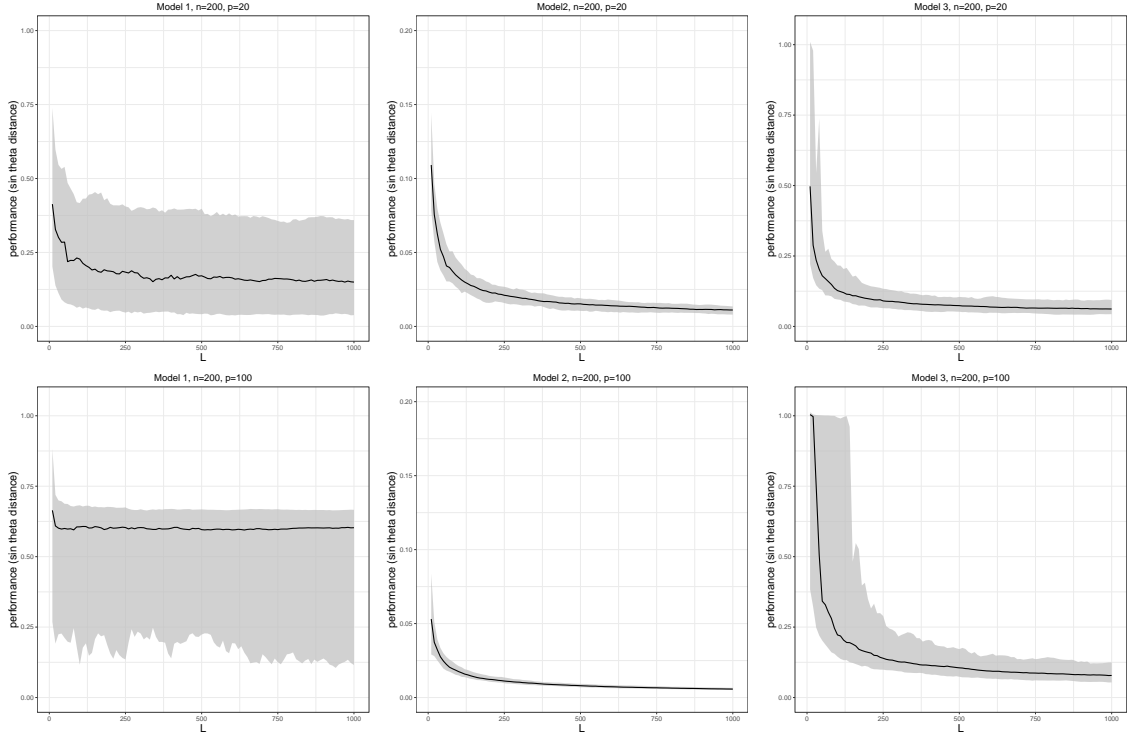


Figure 5: The median (solid line) of the sin-theta distance (see (2)) between $U_{1:d_0}$ from the output of Algorithm 1 and the true direction A_0 over 100 repeats of the simulation as L varies. We present the results for Model 1a (left), Model 2 (middle) and Model 3 (right), for $p = 20$ (top row) and $p = 100$ (bottom row). The grey shaded region shows area between the 5%-95% quantiles for each value of L .

two singular vectors (but this is not captured by the sin theta distance measure presented here). In fact, an extension of our method given in Section 4 is able to find the majority of the signal in a one dimensional projection using a double application of our procedure.

Turning now to the choice of M and d , which together determine the total number of projection directions considered within each of the L groups in Algorithm 1. In slight contrast with the choice of L , there is a trade-off when choosing d and M . For instance, if M is taken to be small (e.g. less than 20 when $p = 20$) then it's unlikely that we have a good projection within a block of size M . On the other hand, if M is taken to be very large (e.g. greater than 1000 when $p = 20$) we may start to overfit, although this effect is often negligible due to the data resampling strategy taken in Algorithm 1. In our experiments we see that the performance of our algorithm levels off as opposed to deteriorating as M increases. Regarding the projection dimension d , if d is taken to be too small, in particular less than (the unknown) d_0 , then we will always miss one or more projection directions, as our algorithm will consistently choose only a more dominant dimension reduction direction. However, we aim to keep d to be relatively small both for computational considerations and the fact that the base regression methods may suffer from the curse of dimensionality.

To explore these aspects in practice, we repeat the experiments presented in Figure 5, but now with L fixed at the default recommendation of 200, and vary $d \in \{1, 2, 5, 10, 20\}$ and $M \in [1000]$. The results are presented in Figure 6. When $p = 20$, we see that taking $d = 1$ is not effective across all three models considered, and there is an advantage in taking $d > d_0$. To elucidate this point, consider an example where $d_0 = 1$. Setting $d = 1$ requires one of the M projections in each group to be relatively highly correlated with the true population direction, which is rare unless M is very large. With a larger d , it is more likely that we find a projection with some signal, which then leads to good performance in the final aggregation step of our algorithm. However, if d is too large, the base method may start to overfit, as seen in, for example, Model 1 when $p = 20$ and $d = 10$.

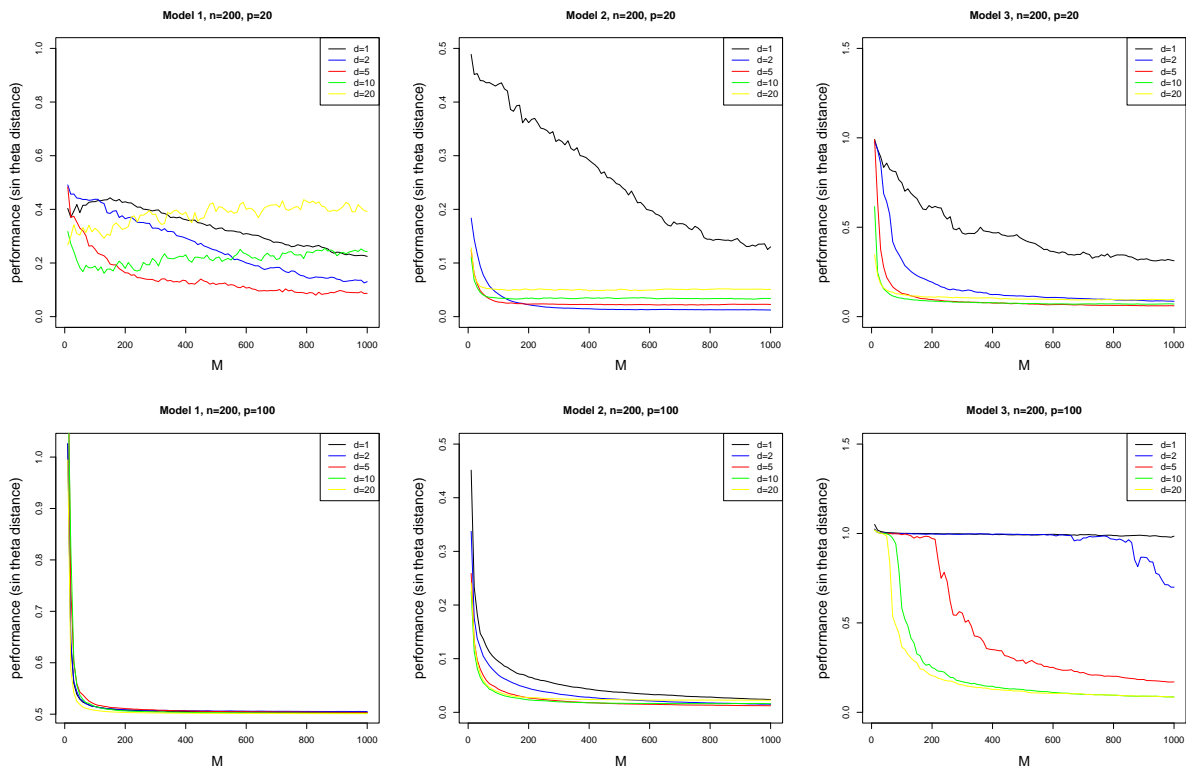


Figure 6: The median of the sin-theta distance (see (2)) between $U_{1:d_0}$ from the output of Algorithm 1 and the true direction A_0 over 100 repeats of the simulation as M varies from 10 to 2000, with $d = 1$ (black), $d = 2$ (blue), $d = 5$ (red), $d = 10$ (green) and $d = 20$ (yellow). We present the results for Model 1a (left), Model 2 (middle) and Model 3 (right), for $p = 20$ (top row) and $p = 100$ (bottom row).

Regarding M , we see that when $p = 20$ and $d = 5$, the performance of our proposal improves rapidly as M increases, but then levels off for M between 100 and 200. When $p = 100$ in Model 1, M needs to be very large in order to capture all signal in the first singular vector of U . In fact, nearly all of the signal is contained in the first two singular vectors of U , even for moderately small values of M . For Model 3, with $p = 100$, the

algorithm finds one of the $d_0 = 2$ directions for small values of M (for every d), but larger d and M are needed to capture the second direction. This explains the two plateaux seen in the curves in bottom right plot. Overall, we recommend taking $d = \lceil \sqrt{p} \rceil$ and $M = 10p$ as a sensible default choices.

3.4 Choice of \hat{d}_0

In some scenarios, the user may have a predetermined lower dimension, \hat{d}_0 say, in mind. In which cases, as mentioned above, they should simply output the first \hat{d}_0 columns of U from the output of Algorithm 1 and set $\hat{A}_0 = (U_1, \dots, U_{\hat{d}_0})$. Indeed, the singular vectors of U , in some sense, represent the most frequently chosen dimensions (in decreasing order of importance) across the groups of projections in the algorithm.

In situations where the desired dimension is unknown, we propose to use the information contained in the singular values D from the output of Algorithm 1. The main idea is to compare these singular values with median of those obtained from applying the corresponding procedure to random projections with the same distribution (i.e. without selection within each group of size M) – see Algorithm 2 below.

Algorithm 2: EDR Dimension Estimator

- 1 **Input:** Projection dimension $d \in [p]$, projection distribution Q on $\mathcal{Q}_{p \times d}$, number of groups L , and the vector $\text{diag}(D) = (D_1, \dots, D_p)$ of singular values from the output of Algorithm 1, as well as a random projection resample size $R \in \mathbb{N}$.
 - 2 Let $\mathbf{P}_{1,1}, \dots, \mathbf{P}_{L,R} \stackrel{\text{i.i.d.}}{\sim} Q$.
 - 3 Set $\hat{\Pi}^{(r)} = \frac{1}{L} \sum_{\ell=1}^L \mathbf{P}_{\ell,r} \mathbf{P}_{\ell,r}^T$, for $r \in [R]$.
 - 4 Calculate the singular value decomposition of $\hat{\Pi}^{(r)} = U^{(r)} D^{(r)} (U^{(r)})^T$ and let $\text{diag}(D^{(r)}) = (D_1^{(r)}, \dots, D_p^{(r)})$.
 - 5 Let $T_j = \frac{1}{R} \sum_{r=1}^R \mathbb{1}_{\{D_j^{(r)} \leq D_j\}}$
 - 6 **Output:** The dimension $\hat{d}_0 := \max\{j \in [p] : T_\ell > 1/2, \text{ for all } \ell \leq j\}$.⁴
-

The motivation behind our approach is that, for a particular direction to be selected, there should be evidence that it contains more signal than expected at random. For the first singular value, this asks that there is a dimension which is more likely to be selected by our algorithm than what happens at random. For later columns of U , since our projections are rescaled to have trace d , we have

$$\sum_{j=1}^p D_j = \text{trace}(\hat{\Pi}) = d.$$

Thus there is a natural penalty to selecting more dimensions in cases where there are relatively large singular values earlier on in D .

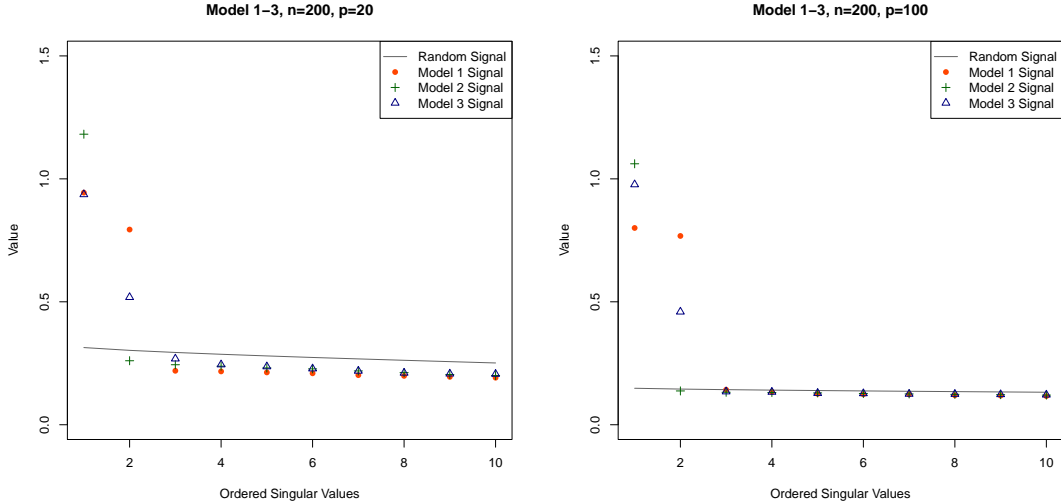


Figure 7: Comparison between the vector D of singular values from the output of Algorithm 1 for Models 1a, 2 and 3, and the median of corresponding $D^{(r)}$ in Algorithm 2 for $p = 20$ (left) and $p = 100$ (right). We present only the first 10 singular values in each case.

Figure 7 demonstrates our procedure for selecting \hat{d}_0 in Models 1a, 2 and 3. For Model 1a, both when $p = 20$ and $p = 100$, the output suggests retaining the first two singular vectors. This is in part because, as also seen in Figure 2, the single signal $\frac{1}{\sqrt{2}}(X_1 + X_2)$ is often split into two. The reason in part due to the fact, even though the projection $(1/\sqrt{2}, -1/\sqrt{2}, 0, \dots, 0)^T$ is orthogonal to the true signal direction, the response Y is not (marginally) independent of $X_1 - X_2$ and therefore our algorithm suggests selecting (approximately) this direction. We demonstrate in Section 4 below how applying our algorithm twice in this cases can accurately estimate only the true one-dimensional signal. For the other two models, there is a clear indication that we should take $\hat{d}_0 = d_0$, namely $\hat{d}_0 = 1$ in Model 2 and $\hat{d}_0 = 2$ in Model 3 and in fact we recover most of the signal here; for example, for Model 2 when $p = 20$ we have $|U_1^T e_3| > 0.999$ and for Model 3, we have $\min\{|U_1^T e_6|, |U_2^T e_7|\} \geq 0.995$. We delay further evaluation of the this approach to selecting \hat{d}_0 to our full simulation study in Section 5.

3.5 Computational considerations

The majority of the computational cost of our main algorithm arises from the fact that the base regression method is applied $L \cdot M$ times. Moreover, the cost of applying the base method generally depends on the projection dimension d and the sample size n_1 . If the ambient dimension p is relatively modest (i.e. in the hundreds), the cost of projecting the data and performing the final singular value decomposition is relatively low. Notably, the $L \cdot M$ applications of the base regression method can be parallelised, meaning that the overall computational burden can be significantly reduced if high-performance computing resources are available.

Assessing the full trade off in computational resources and statistical performance in selecting the inputs to Algorithm 1 discussed in this section is beyond the scope of the work here. Nevertheless in Section B.1 we show that the runtime of our algorithm, while slower than the competitors considered, is manageable with our recommended settings even when p and n are large.

4 Double random projection ensemble dimension reduction

In this section, we explore how applying our main algorithm a second time may help to further reduce the dimension in cases where the used is not satisfied with the suggested dimension from an initial application of Algorithms 1 and 2. For example, we may have knowledge of the true dimension d_0 , but Algorithm 2 suggests $\hat{d}_0 > d_0$. In other cases, we may not know the true d_0 precisely, but may still have a specific target dimension in mind.

We will demonstrate that this double application strategy is particularly effective when the number of covariates contributing to $\mathcal{S}(A_0)$ outnumber the true dimension d_0 . In particular, in such situations, a single application of our algorithm may favour the coordinate axes of the relevant covariates, but fail to combine these effectively into the smallest possible number of dimension reduction directions. One perspective of this approach, is that the first application of our algorithm acts as a screening step to select potentially relevant directions, while the second application then combines these directions to yield a lower dimensional projection that still retains a large amount of the signal. The full procedure is presented in Algorithm 3.

Algorithm 3: Double RPE dimension reduction

- 1 **Input:** Data $((x_1, y_1), \dots, (x_n, y_n)) \in (\mathbb{R}^p \times \mathbb{R})^n$ and desired dimension $\check{d}_0 \in [p]$.
 - 2 Let U and D be the output of Algorithm 1 applied to $(x_1, y_1), \dots, (x_n, y_n)$ with $L = 200$, $M = 10p$, $d = \lceil \sqrt{p} \rceil$, $n_1 = \lceil 2n/3 \rceil$, $Q = \frac{1}{2}Q_C^{\otimes d} + \frac{1}{2}Q_N^{\otimes d}$, and $\hat{g} = \hat{g}_{\text{MARS}}$.
 - 3 Let \hat{d}_0 be the output of Algorithm 2 applied to D , with $L = 200$, $d = \lceil \sqrt{p} \rceil$, $Q = \frac{1}{2}Q_C^{\otimes d} + \frac{1}{2}Q_N^{\otimes d}$.
 - 4 **if** $\hat{d}_0 > \check{d}_0$ **then**
 - 5 Set $\hat{A}_0 := (U_1, \dots, U_{\hat{d}_0})$ and $z_i := \hat{A}_0^T x_i$ for $i \in [n]$.
 - 6 Let \check{U} and \check{D} be the output of Algorithm 1 applied to $(z_1, y_1), \dots, (z_n, y_n)$ with $L = 200$, $M = 10\hat{d}_0$, $d = \lceil \sqrt{\hat{d}_0} \rceil$, $n_1 = \lceil 2n/3 \rceil$, $Q = \frac{1}{2}Q_C^{\otimes d} + \frac{1}{2}Q_N^{\otimes d}$, and $\hat{g} = \hat{g}_{\text{MARS}}$.
 - 7 Let $\check{A}_0 = \hat{A}_0(\check{U}_1, \dots, \check{U}_{\check{d}_0}) \in \mathbb{R}^{p \times \check{d}_0}$
 - 8 **else**
 - 9 Let $\check{A}_0 = (U_1, \dots, U_{\check{d}_0}) \in \mathbb{R}^{p \times \check{d}_0}$
 - 10 **Output:** The projection \check{A}_0 .
-

We demonstrate this procedure using Model 1a and a new model as follows:

- Model 4: Let $X = (X_1, \dots, X_p)^T \sim N_p(0, I)$ and

$$Y = \exp\left(\frac{X_1 - X_2 + X_3}{3}\right) + \epsilon$$

with $\epsilon \sim N(0, 1/5)$ independent of X . Here $A_0 = \frac{1}{\sqrt{3}}(1, -1, 1, \mathbf{0}_{p-3})^T$ is 1-dimensional.

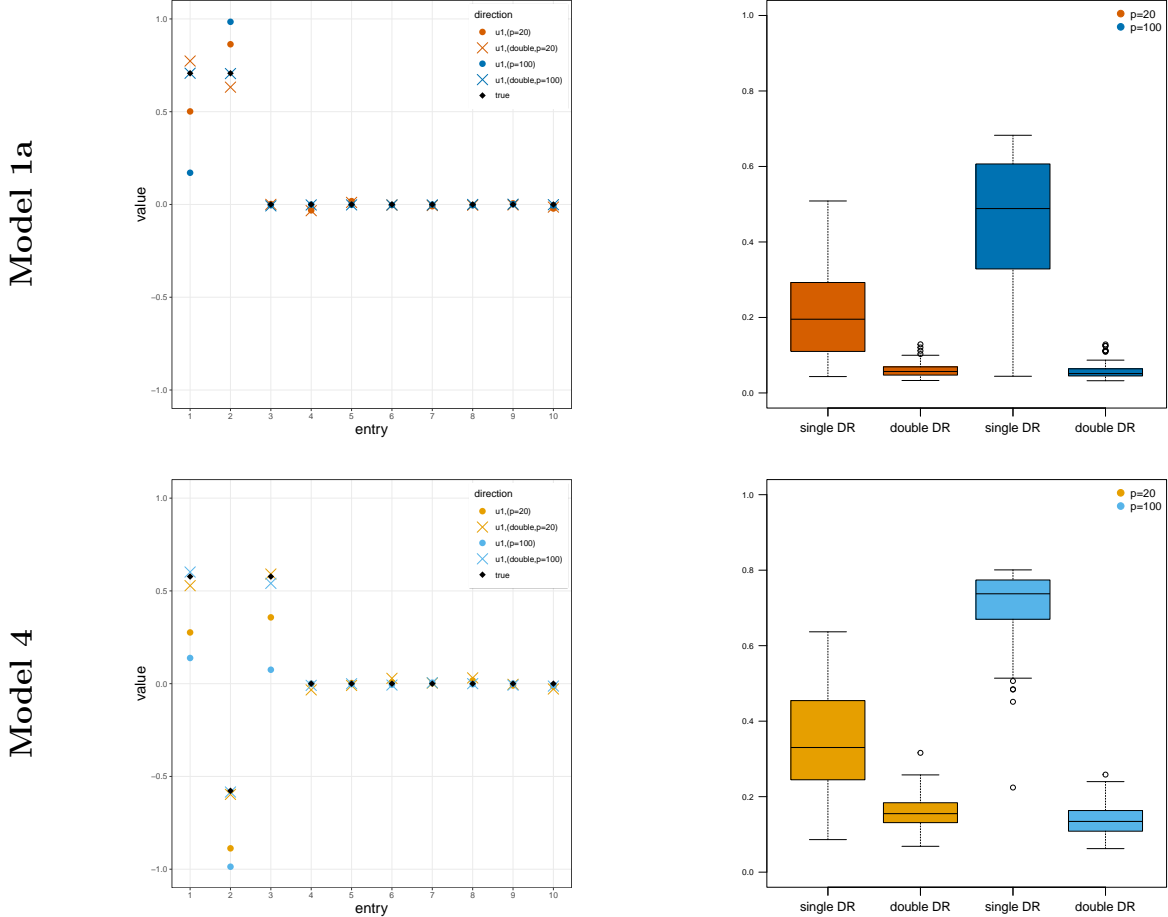


Figure 8: Demonstration of our Double RPE dimension reduction approach in Algorithm 3. We compare the results of a single application of our Algorithm 1 taking $\hat{d}_0 = 1$, with double application in Algorithm 3 with $\hat{d}_0 = 1$. We present the first 10 entries of the estimated A_0 for a single run of the experiment (left) alongside the sin-theta distance (right) over 100 repeats of the experiment. We have $p \in \{20, 100\}$ and Model 1a (top) and Model 4 (bottom).

In both Models 1a and 4, the true projection A_0 is one-dimensional and therefore we seek to find the best one dimensional projection based on our algorithms. Figure 8 shows the comparison between the leading singular vector from the output of Algorithm 1 and

the output of Algorithm 3 with default recommendation inputs and with $\check{d}_0 = 1$. More precisely, we apply Algorithm 1 with the recommended values from the previous section, that is $L = 200$, $M = 10p$, $d = \lceil \sqrt{p} \rceil$, $n_1 = \lceil 2n/3 \rceil$, $Q = \frac{1}{2}Q_C^{\otimes d} + \frac{1}{2}Q_N^{\otimes d}$ for the projection distribution, and $\hat{g} = \hat{g}_{\text{MARS}}$. In both models, a second application of our algorithm leads to significantly improved performance. In Model 1a, the first application of Algorithm 1 typically identifies that the first two variables are important, but splits this signal across the first two singular vectors. The second application then effectively combines these separate signals into a better estimator of the one-dimensional A_0 . A similar scenario occurs in Model 4, though the improvement is slightly less pronounced.

In cases where the initial application of Algorithms 1 and 2 correctly identify the true dimension d_0 , then there is no benefit to be gained from applying Algorithm 3. However, as long as $\check{d}_0 \geq d_0$, there is typically no disadvantage either – see, for example the results for Model 3 presented in Figure 9.

5 Numerical simulations

In this section, we present the results of a large simulation study comparing the performance of our proposal with several existing methods for estimating the central mean subspace $\mathcal{S}(A_0)$. We evaluate the performance of three slightly different versions of our proposed method. The first variant applies Algorithm 1 on its own, and the second variant is the double dimension reduction approach presented in Algorithm 3. Both variants are suitable when the true projection dimension d_0 is known. The third variant, which combines Algorithm 1 and 2, is designed for situations where d_0 is unknown. For comparison, we use the default implementations of several existing methods, including SIR (Li, 1991), pHd (Li, 1992), MAVE (Xia et al., 2002), DR (Li and Wang, 2007), gKDR (Fukumizu and Leng, 2014) and drMARS (Liu et al., 2023). The models used in our experiments include Models 1a, 2, 3 and 4, introduced earlier in the paper, as well as five additional models as follows: let $X := (X_1, \dots, X_p)^T \sim N_p(0, I)$ and $\epsilon \sim N(0, 1/4)$, with X and ϵ independent. The additional models are specified as:

- Model 5: $Y = \frac{X_1 + X_2 + 5e^{-2(X_1 + X_2 + X_3)^2}}{2} + \epsilon$,
- Model 6: $Y = 5X_1X_2X_3 + \epsilon$
- Model 7: $Y = 4(X_1 - X_2 + X_3) \sin\left(\frac{\pi}{2}(X_1 + X_2)\right) + \epsilon$
- Model 8: $Y = X_1(X_1 + X_2 + 1) + \epsilon$
- Model 9: $Y = 10 \cos(6X_1) + e^{X_2+1} + \epsilon$

Models 5, 6 and 7 were used by (Liu et al., 2023) in their simulation study, and Model 8 was used in (Li, 1991; Xia et al., 2002; Liu et al., 2023).

In our full simulation study, the results of which are presented in Section B in the Appendix, we vary $n \in \{50, 200, 500\}$ and $p \in \{20, 50, 100\}$ for each model. In the main

text, we focus on the performance when $n = 200$ and $p = 50$, and note that the results are broadly similar across the different values of n and p considered.

5.1 Dimension d_0 known

We begin with the slightly simpler scenario where the dimension d_0 of the central mean subspace $\mathcal{S}(A_0)$ is known. In this case, our first proposal, denoted as **RPE** in Figure 9 below, sets $\hat{A}_0 = (U_1, \dots, U_{d_0})$, where $U = (U_1, \dots, U_p)$ is the output of Algorithm 1 with the default inputs recommended in Section 3. In particular, we set $d = \lceil p^{1/2} \rceil$, $L = 200$, $M = 10p$, $n_1 = \lceil 2n/3 \rceil$, $Q = \frac{1}{2}Q_C^{\otimes d} + \frac{1}{2}Q_N^{\otimes d}$, and $\hat{g} = \hat{g}_{\text{MARS}}$. We also present the performance of Algorithm 3 with $\check{d}_0 = d_0$, which is denoted **RPE2** in Figure 9.

For the competing methods, we use the R packages `dr` (Weisberg, 2002) for SIR and pHd, `MAVE` (Hang and Xia, 2021) for MAVE, and the relevant code available via gitHub for `DR` (https://github.com/JSongLab/SDR_HC), `gKDR` and `drMARS` (<https://github.com/liuyu-star/drMARS>). In each case, we use the corresponding default recommendations to select appropriate tuning parameters.

Figure 9 presents boxplots of the sin-theta distance $d_F(\mathcal{S}(\hat{A}_0), \mathcal{S}(A_0))$ across 100 repeats of the experiment for the nine models. We observe that both our RPE and RPE2 approaches are highly effective. In Models 1a and 4, RPE2 demonstrates a clear improvement over RPE, as we’ve also highlighted in Section 4. For the other models, a single application of our Algorithm 1 performs very well. The `drMARS` approach is also competitive in Models 1a, 5, 6 and 7. The other competitors suffer prohibitively due to the curse of dimensionality and are typically ineffective in the 50-dimensional examples shown here⁵. There are a few cases where the performance our methods (and in fact all approaches considered here) does not achieve a sin-theta distance close to zero. In Models 5 and 7, our algorithm tends to find the space spanned by e_1 and e_2 , but misses the weak signal in the e_3 direction. Model 6 is particularly challenging, both because in order to obtain a non-trivial prediction of the response Y , we need some knowledge of all three covariates X_1, X_2 and X_3 , (indeed, for example, $\mathbb{E}(Y|(X_1, X_2)) = 0$) and, even given an oracle projection into the subspace spanned by e_1, e_2 and e_3 , the base regression problem remains difficult. We observe better performance in these models when $p = 20$ and $n = 500$ – see Section B.

5.2 Dimension d_0 unknown

We now turn to the more challenging, and arguably more realistic scenario where d_0 is unknown. In this subsection, our primary goal is to evaluate the performance of our Algorithm 1 when the dimension of the final projection \hat{d}_0 is chosen using Algorithm 2. In this case, we focus solely on the performance of a single application of our random projection ensemble algorithm. The double dimension reduction technique in Algorithm 3 is not considered here, as it requires a desired projection dimension to be prespecified. For

⁵The performance of these approaches is better in lower dimensional settings, though our random projection based methods still offer an improvement when $p = 20$ – see the full results in Section B.

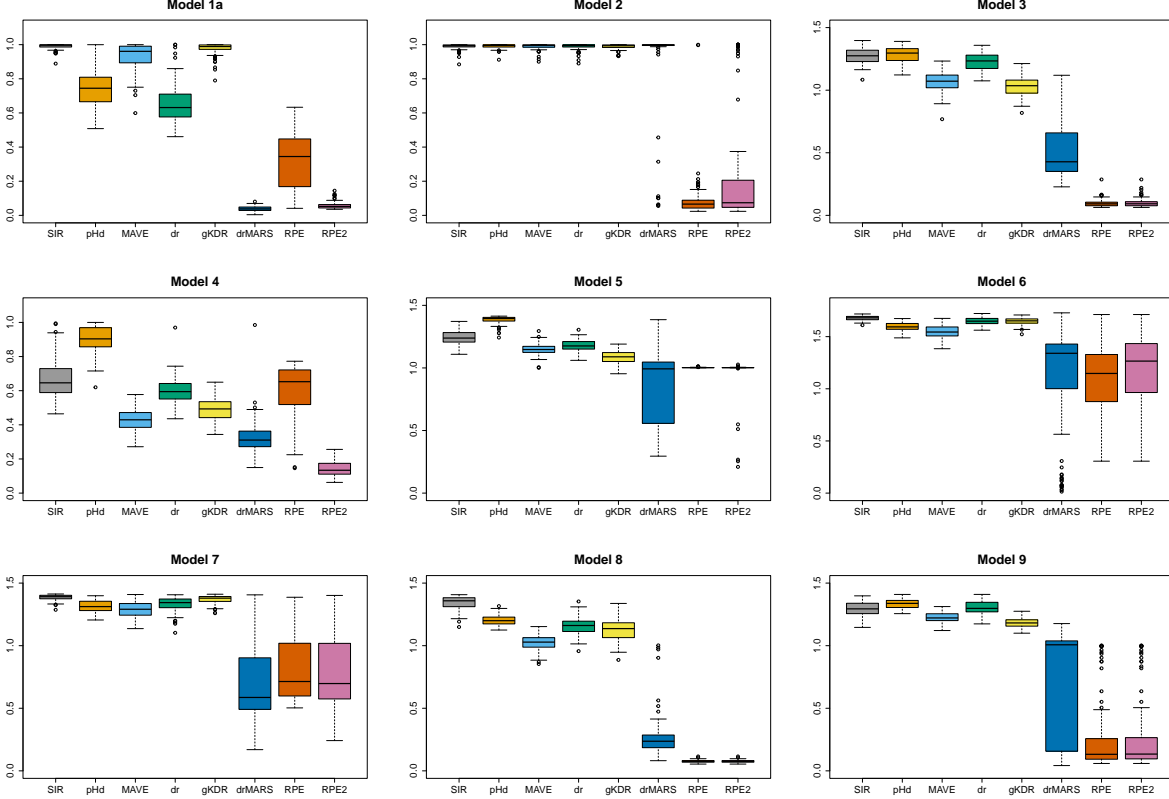


Figure 9: Boxplots of $\sin \theta$ distance between the subspaces spanned by the estimated projection \hat{A}_0 and true projection A_0 for our random projection based methods and the six competing methods when d_0 is known. We present the results for models 1a-9 over 100 repeats of the experiment, with $n = 200$ and $p = 50$.

comparison, we also include the results from the competing methods, where the dimension is chosen using the corresponding recommended default approaches. Specifically, these are the *marginal dimension test* from the R package `dr` for SIR and pHd; and *generalised cross-validation*, which is available as part of the `mave` package (for MAVE), and the corresponding gitHub links given in the previous subsection (for gKDR and drMARS⁶). The DR method is only applicable with a prespecified d_0 and hence it is excluded from this subsection.

In our experiments below, we will reuse the Models 1a through 9 described earlier. For our proposal, labelled **RPE** in the boxplots below, follows the recommendations from Section 3 for Algorithm 1, with \hat{d}_0 selected via Algorithm 2 using $R = 10000$. Competing methods utilize their respective default values for any tuning parameters.

The results in Figure 10 show that, with the exception of SIR and pHd, most methods including ours tend to be somewhat liberal in choosing \hat{d}_0 , in the sense that they typically take \hat{d}_0 to be larger than d_0 . Conversely, SIR and pHd typically selects $\hat{d}_0 = 0$ in these

⁶for these two methods, we set the maximum projection dimension to be $\lceil \sqrt{p} \rceil$

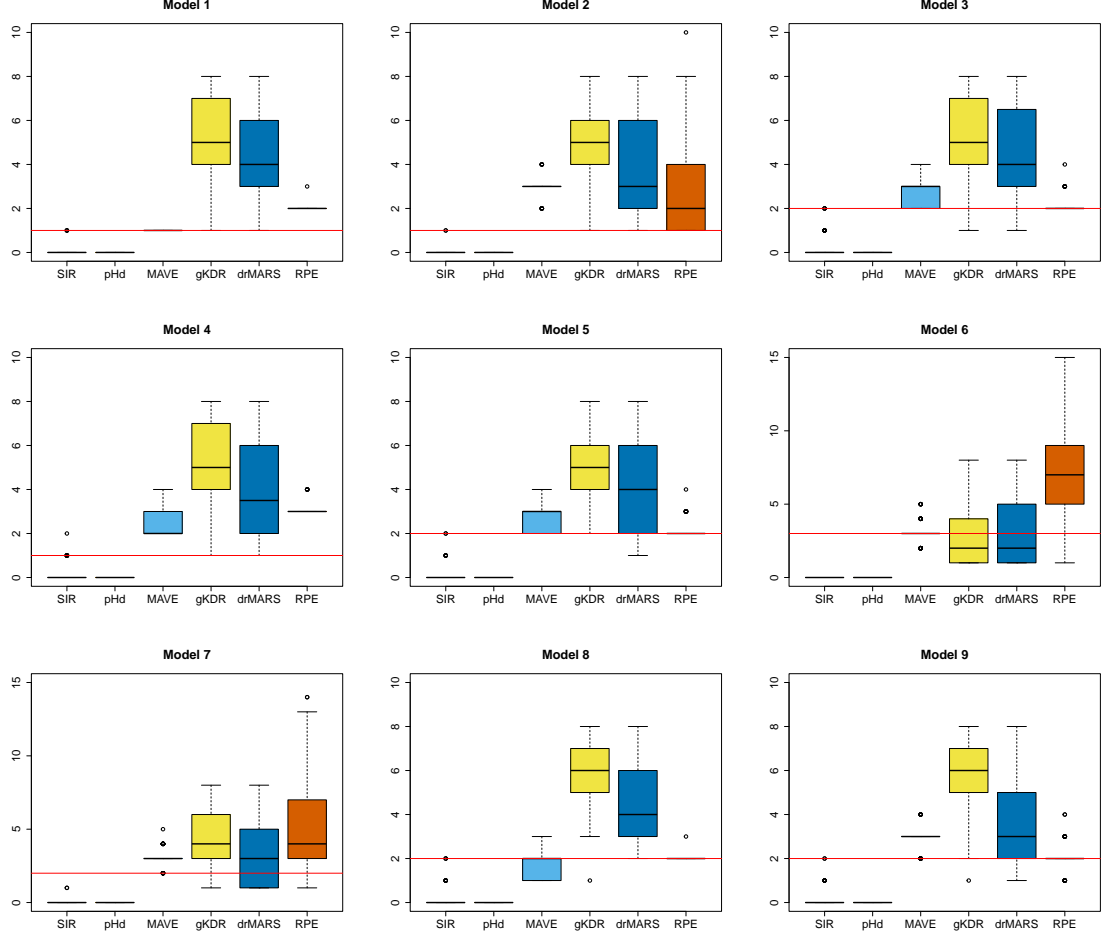


Figure 10: Boxplots of \hat{d}_0 from Algorithm 2 alongside the competing methods over 100 repeats of the simulation for models 1a-9. We present the results for $n = 200$ and $p = 50$. The red horizontal lines show the dimension d_0 of the true A_0 .

examples, indicating no signal found – as mentioned above, both methods appear to be suffering from the curse of dimensionality.

To further assess the performance when d_0 is unknown, we introduce two additional evaluation metrics, which measure the *false positives* and *false negatives*:

$$d_{\text{FP}}(\hat{A}_0, A_0) := \|(I - A_0 A_0^T) \hat{A}_0\|_F \quad (4)$$

$$d_{\text{FN}}(\hat{A}_0, A_0) := \|(I - \hat{A}_0 \hat{A}_0^T) A_0\|_F \quad (5)$$

In both cases, \hat{A}_0 is a $p \times \hat{d}_0$ dimensional projection, where \hat{d}_0 need not be equal to d_0 . The metric d_{FP} measures *false positives*, in the sense that it quantifies the extent to which \hat{A}_0 contains regions of the ambient p dimensional space that are orthogonal to A_0 . In particular, if $\mathcal{S}(\hat{A}_0) \subseteq \mathcal{S}(A_0)$, then $d_{\text{FP}}(\hat{A}_0, A_0) = 0$. In contrast, d_{FN} measures *false negatives* and

quantifies the amount of the space spanned by A_0 that is *missed* by the projection \hat{A}_0 . Indeed, we have $d_{\text{FN}}(\hat{A}_0, A_0) = 0$ when $\mathcal{S}(A_0) \subseteq \mathcal{S}(\hat{A}_0)$. Broadly speaking, increasing \hat{d}_0 will typically decrease d_{FN} at the expense of increasing d_{FP} . Only when $\hat{d}_0 = d_0$ can both d_{FP} and d_{FN} be equal to (or close to) zero.

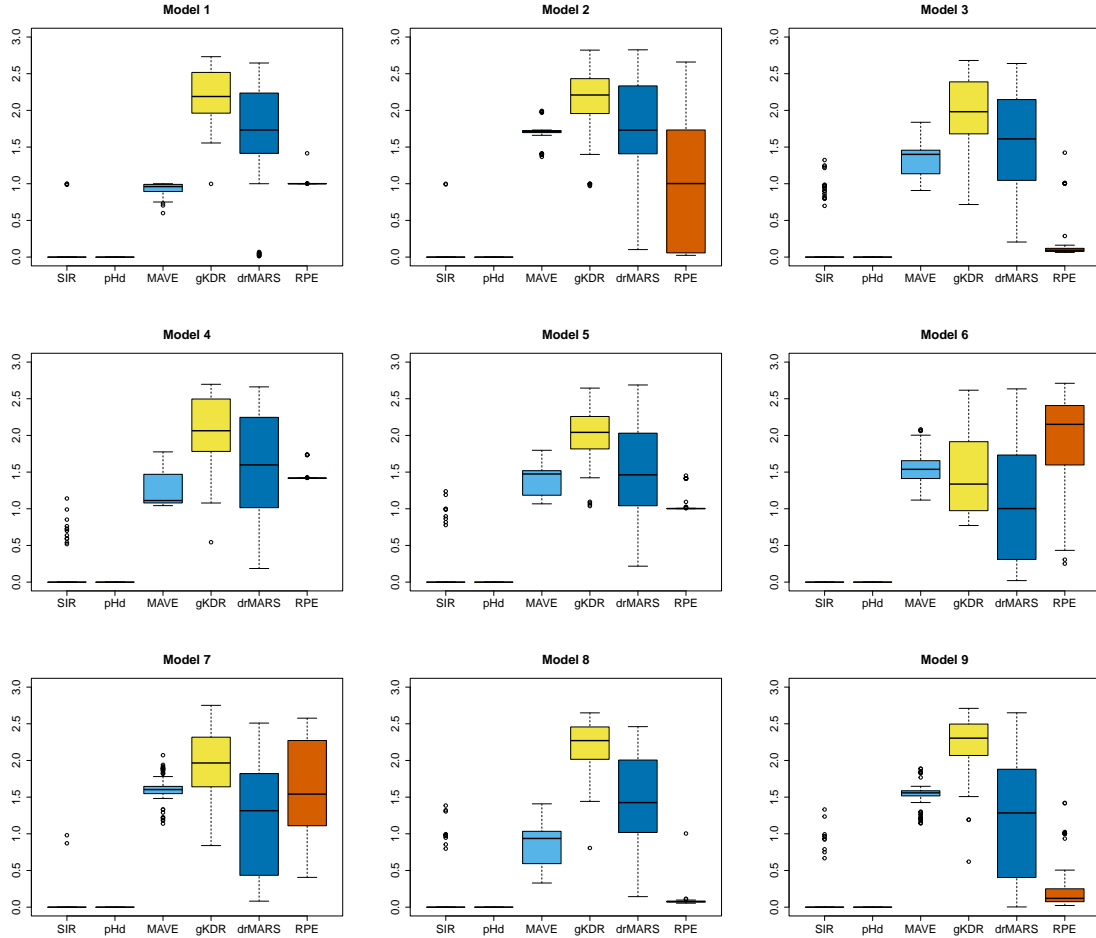


Figure 11: Boxplots of $d_{\text{FP}}(\hat{A}_0, A_0)$ for the different methods when d_0 is unknown for models 1a-9 over 100 simulations. Our RPE method here is based on the output from Algorithm 1, with the corresponding projection dimension \hat{d}_0 chosen via Algorithm 2. For the competing methods, \hat{d}_0 is chosen via the corresponding approach described at the beginning of this subsection. The presented setting is $n = 200$, $p = 50$.

Figures 11 and 12 present results of d_{FP} and d_{FN} , respectively, for different methods across the nine models. In cases where \hat{d}_0 is frequently selected to be d_0 , namely Models 3, 8 and 9, we observe excellent performance in terms of both false positives and false negatives. In Models 1 and 4, our algorithm tends to identify the one-dimensional signal direction, by selecting the individual coordinate axes that contribute to the true projection. In these cases, we perform well in terms of the false negative measure, indicating that nearly all of

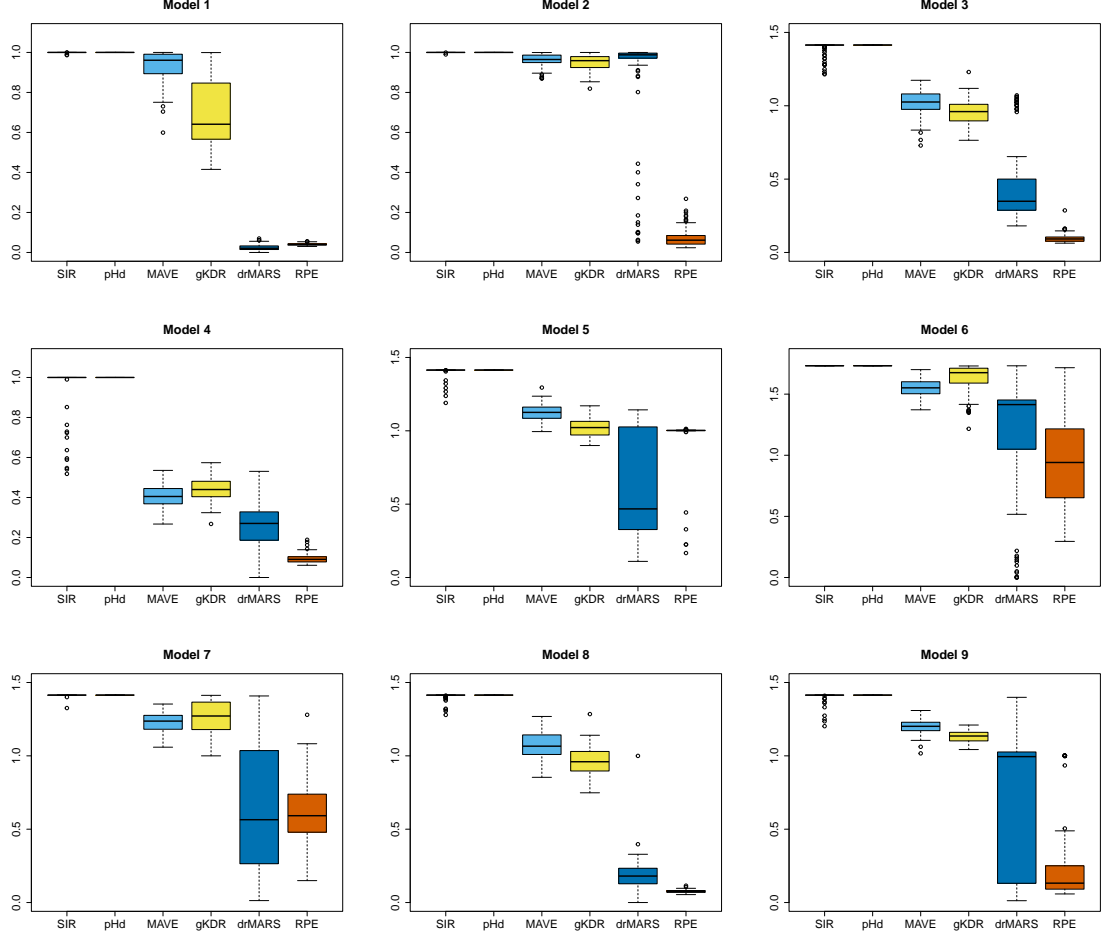


Figure 12: Boxplots of $d_{\text{FN}}(\hat{A}_0, A_0)$ for the different methods when d_0 is unknown for models 1a-9 over 100 simulations. Our RPE method here is based on the output from Algorithm 1, with the corresponding projection dimension \hat{d}_0 chosen via Algorithm 2. For the competing methods, \hat{d}_0 is chosen via the corresponding approach described at the beginning of this subsection. The presented setting is $n = 200$, $p = 50$.

the signal is captured. However, this comes at the cost of higher false positives, though our approach remains competitive with the other methods considered. For Models 2 and 6, we take \hat{d}_0 to be larger d_0 , and thus include some noise directions alongside the signals. However, our approach still excels in terms of false negatives, outperforming the other methods considered, especially in Model 2, where the competing methods fail to capture the signal directions. In Model 6 we pay a price in terms of false positives for this advantage. Finally, in Models 5 and 7, our algorithms tends to select the e_1 and e_2 directions separately, while missing e_3 , and thus also fails to combine these signals in the optimal way. As a result, both the false positive and false negative performance are not close to zero. Nevertheless, our method remains competitive with the other algorithms considered in these examples.

6 Real world application

In this section, we compare the performance of our methods with competing approaches using real-world data. We make use of the following four datasets from the UC Irvine Machine Learning Repository:

1. **Superconductivity**⁷ (Hamidieh, 2018): This dataset consists of measurements on 81 physical and atomic covariates for 21263 superconductors. The response variable is the critical temperature of the superconductor. We use all $p = 81$ covariates and randomly select a subsample of size $n = 1000$ observations for training, and the remainder used for testing.
2. **Communities and Crime**⁸ (Redmond and Baveja, 2002): This dataset consists of 1994 observations on 122 predictive variables relating to socioeconomic and police data. The response variable of interest is per capita rate of violent crimes. For simplicity, we remove variables with missing values, leaving $p = 105$ predictive covariates in our experiment and we take a random sample of $n = 1329$ observations for training.
3. **Residential Building**⁹ (Rafei and Adeli, 2016): This dataset includes construction cost, sales prices, project variables, and economic variables corresponding to real estate single-family residential apartments in Tehran, Iran. There are 372 observations of 105 variables in total. We use all $p = 105$ predictive variables and take a random sample of $n = 248$ observations for training. There are two options for the response variable, either sales price or construction cost, both options are included in our experiments.
4. **Geographical Origin of Music**¹⁰ (Zhou et al., 2014): This dataset consists of 1059 observations on 116 variables relating to audio features of a piece of music. We use the latitude of the piece’s origin as the response variable. In this case all $p = 116$ variables are used, and a subsample of $n = 706$ observations is taken for training.

In this section’s experiments, since the true projection A_0 is unknown, we measure the performance of the different techniques based on regression prediction accuracy after projecting the data. More precisely, we fixed the projection dimension \hat{d}_0 , set to either 3 or 10, and then apply the methods described in Section 5.1 using only the training data. The interpretation is that we select the \hat{d}_0 most important directions chosen by each method. We then apply MARS¹¹ to the projected training data after each method. The performance is measured using the root-mean-squared-error (RMSE) on the corresponding projected test set. The results of our real data experiments are presented in Table 1, where we see that our methods enjoy competitive performance across all four datasets considered here.

⁷<https://archive.ics.uci.edu/dataset/464/superconductivity+data>

⁸<https://archive.ics.uci.edu/dataset/183/communities+and+crime>

⁹<https://archive.ics.uci.edu/dataset/437/residential+building+data+set>

¹⁰<https://archive.ics.uci.edu/dataset/315/geographical+original+of+music>

¹¹We use cross-validation to determine the degree, with the maximum order of interactions set to four.

Dataset	No proj	\hat{d}_0	Dimension reduction technique						Our Methods	
			SIR	pHd	MAVE	DR	gKDR	drMARS	RPE	RPE2
1	17.4	3	16.5	30.2	19.3	29.9	18.1	18.8	19.4	17.5
		10	17.3	27.8	18.0	22.2	17.9	20.4	17.1	17.1
2	0.180	3	0.127	0.212	0.140	0.184	0.132	0.138	0.129	0.129
		10	0.137	0.187	0.135	0.136	0.132	0.140	0.132	0.126
3(sales)	150	3	295	1198	218	/	386	158	218	218
		10	295	699	295	/	429	211	124	124
3(cons.)	32.1	3	70.4	203	47.6	/	161	136	34.7	34.7
		10	68.4	301	42.4	/	47.1	29.6	24.1	24.1
4	25.7	3	16.9	18.1	16.7	/	17.7	17.0	16.9	16.1
		10	17.9	17.5	15.8	/	17.0	19.4	17.0	16.0

Table 1: The RMSE on the test set for our real data experiments. For comparison, we include the corresponding results when we apply the MARS algorithm directly to the original data in the ambient space (i.e. without projecting the data first). For datasets 3 and 4 the DR method had very large RMSE and we therefore omitted the results.

7 Discussion and extensions

We have introduced a new general approach to sufficient dimension reduction, based on aggregating an ensemble of carefully chosen projections. The proposed framework is highly flexible, allowing for different distributions of random projections and a user-specified choice of base regression method. We provide default recommendations for these aspects based on extensive numerical experiments, but we anticipate that many other possible choices will be effective in certain cases.

There are several ways in which our framework could be extended further. First, a natural assumption in high-dimensional settings is sparsity, specifically the case where the projection A_0 is sparse (i.e. contains many zero entries). In this scenario, it may be more effective to consider sparse random projections, but perhaps more importantly, we'd suggest that employing sparse singular value decomposition (see, for example, [Yang et al., 2014](#)) to aggregate the chosen projections in order to ensure the resulting estimate \hat{A}_0 is sparse.

A second possible extension arises in the context of additive index models (see, for example, [Friedman and Stuetzle, 1981](#); [Ruan and Yuan, 2010](#)). In this case, we may seek to sequentially find the signal directions one-by-one. For the first signal direction, we could apply our Algorithm 1 directly, keeping only the first singular vector. To identify the subsequent signal directions, we would then apply a modification of our algorithm that always includes the signals found so far and considers random projections that are orthogonal to the previously identified signals.

Finally, while this paper has focused on dimension reduction, specifically estimating the projection matrix A_0 , it would be interesting to consider alternative ways of aggregating the results when the primary objective is to predict the response Y . In particular, improved predictive performance might be achieved by directly aggregating the predictions from the

chosen projections, as opposed to fitting a new regression model after projecting the data with our estimated projection \hat{A}_0 . These extensions are left for future work.

Acknowledgements

The research of TIC was supported by Engineering and Physical Sciences Research Council (EPSRC) New Investigator Award EP/V002694/1.

References

- Adraghi, K. P. and Cook, R. D. (2009). Sufficient dimension reduction and prediction in regression. *Philosophical Transactions of the Royal Society A: Mathematical, Physical and Engineering Sciences*, 367(1906):4385–4405.
- Ahfock, D. C., Astle, W. J., and Richardson, S. (2021). Statistical properties of sketching algorithms. *Biometrika*, 108(2):283–297.
- Anderlucci, L., Fortunato, F., and Montanari, A. (2022). High-dimensional clustering via random projections. *Journal of Classification*, 39:191—216.
- Banijamali, E., Karimi, A.-H., and Ghodsi, A. (2018). Deep variational sufficient dimensionality reduction. *Third workshop on Bayesian Deep Learning (NeurIPS 2018)*.
- Bell, C. G., Lowe, R., Adams, P. D., Baccarelli, A. A., Beck, S., Bell, J. T., Christensen, B. C., Gladyshev, V. N., Heijmans, B. T., Horvath, S., et al. (2019). DNA methylation aging clocks: challenges and recommendations. *Genome Biology*, 20:1–24.
- Bingham, E. and Mannila, H. (2001). Random projection in dimensionality reduction: applications to image and text data. In *Proceedings of the Seventh ACM SIGKDD International Conference on Knowledge Discovery and Data Mining*, KDD '01, page 245–250, New York, NY, USA. Association for Computing Machinery.
- Cannings, T. I. (2021). Random projections: Data perturbation for classification problems. *Wiley Interdisciplinary Reviews: Computational Statistics*, 13(1):e1499.
- Cannings, T. I. and Samworth, R. J. (2017). Random-projection ensemble classification. *Journal of the Royal Statistical Society, Series B (with discussion)*, 79(4):959–1035.
- Cook, R. D. and Li, B. (2002). Dimension reduction for conditional mean in regression. *The Annals of Statistics*, 30(2):455–474.
- Cook, R. D., Li, B., and Chiaromonte, F. (2007). Dimension reduction in regression without matrix inversion. *Biometrika*, 94(3):569–584.

- Cook, R. D. and Weisberg, S. (1991). Sliced inverse regression for dimension reduction: Comment. *Journal of the American Statistical Association*, 86(414):328–332.
- Dasgupta, S. and Gupta, A. (2003). An elementary proof of a theorem of Johnson and Lindenstrauss. *Random Structures & Algorithms*, 22(1):60–65.
- Davis, C. and Kahan, W. M. (1970). The rotation of eigenvectors by a perturbation. iii. *SIAM Journal on Numerical Analysis*, 7(1):1–46.
- Dobriban, E. and Liu, S. (2019). Asymptotics for sketching in least squares regression. *Advances in Neural Information Processing Systems*, 32.
- Fern, X. Z. and Brodley, C. E. (2003). Random projection for high dimensional data clustering: A cluster ensemble approach. In *Proceedings of the 20th international conference on machine learning (ICML-03)*, pages 186–193.
- Fertl, L. and Bura, E. (2022). Conditional variance estimator for sufficient dimension reduction. *Bernoulli*, 28(3):1862–1891.
- Friedman, J. H. (1991). Multivariate Adaptive Regression Splines. *The Annals of Statistics*, 19(1):1 – 67.
- Friedman, J. H. and Stuetzle, W. (1981). Projection pursuit regression. *Journal of the American statistical Association*, 76(376):817–823.
- Fukumizu, K. and Leng, C. (2014). Gradient-based kernel dimension reduction for regression. *Journal of the American Statistical Association*, 109(505):359–370.
- Gataric, M., Wang, T., and Samworth, R. J. (2020). Sparse principal component analysis via axis-aligned random projections. *Journal of the Royal Statistical Society, Series B*, 82(2):329–359.
- Ghojogh, B., Ghodsi, A., Karray, F., and Crowley, M. (2021). Sufficient dimension reduction for high-dimensional regression and low-dimensional embedding: Tutorial and survey. *arXiv preprint arXiv:2110.09620*.
- Hamidieh, K. (2018). A data-driven statistical model for predicting the critical temperature of a superconductor. *Computational Materials Science*, 154:346–354.
- Hampel, F. R. (1968). *Contributions to the Theory of Robust Estimation*. University of California, Berkeley.
- Hang, W. and Xia, Y. (2021). *MAVE: Methods for Dimension Reduction*. R package version 1.3.11.
- Hoerl, A. E. and Kennard, R. W. (1970). Ridge regression: Biased estimation for nonorthogonal problems. *Technometrics*, 12(1):55–67.

- Horn, R. A. and Johnson, C. R. (2012). *Matrix Analysis*. Cambridge University Press.
- Horvath, S. (2013). DNA methylation age of human tissues and cell types. *Genome Biology*, 14(10):1–20.
- Huang, Z., Kabán, A., and Reeve, H. (2024). Efficient learning with projected histograms. *Data Mining and Knowledge Discovery*, pages 1–53.
- Johnson, W. B. and Lindenstrauss, J. (1984). Extensions of Lipschitz maps into a Hilbert space. *Contemp. Math*, 26(189-206):2.
- Kapla, D., Fertl, L., and Bura, E. (2022). Fusing sufficient dimension reduction with neural networks. *Computational Statistics & Data Analysis*, 168:107390.
- Li, B. and Wang, S. (2007). On directional regression for dimension reduction. *Journal of the American Statistical Association*, 102(479):997–1008.
- Li, K.-C. (1991). Sliced inverse regression for dimension reduction. *Journal of the American Statistical Association*, 86(414):316–327.
- Li, K.-C. (1992). On principal hessian directions for data visualization and dimension reduction: Another application of Stein’s lemma. *Journal of the American Statistical Association*, 87(420):1025–1039.
- Li, L. and Nachtsheim, C. J. (2006). Sparse sliced inverse regression. *Technometrics*, 48(4):503–510.
- Li, P., Hastie, T. J., and Church, K. W. (2007). Nonlinear estimators and tail bounds for dimension reduction in l1 using cauchy random projections. *Journal of Machine Learning Research*, 8(83):2497–2532.
- Liu, Y., Li, D., and Xia, Y. (2023). Dimension reduction and MARS. *Journal of Machine Learning Research*, 24(309):1–30.
- Lopes, M., Jacob, L., and Wainwright, M. J. (2011). A more powerful two-sample test in high dimensions using random projection. In Shawe-Taylor, J., Zemel, R., Bartlett, P., Pereira, F., and Weinberger, K., editors, *Advances in Neural Information Processing Systems*, volume 24. Curran Associates, Inc.
- Ma, Y. and Zhu, L. (2012). A semiparametric approach to dimension reduction. *Journal of the American Statistical Association*, 107(497):168–179.
- Ma, Y. and Zhu, L. (2013). A review on dimension reduction. *International Statistical Review*, 81(1):134–150.
- Marzetta, T. L., Tucci, G. H., and Simon, S. H. (2011). A random matrix-theoretic approach to handling singular covariance estimates. *IEEE Transactions on Information Theory*, 57(9):6256–6271.

- Milborrow, S. (2024). *earth: Multivariate Adaptive Regression Splines*. R package version 5.3.3.
- Rafiei, M. H. and Adeli, H. (2016). A novel machine learning model for estimation of sale prices of real estate units. *Journal of Construction Engineering and Management-asce*, 142:04015066.
- Ramirez, A. B., Arce, G. R., Otero, D., Paredes, J.-L., and Sadler, B. M. (2012). Reconstruction of sparse signals from ℓ_1 dimensionality-reduced cauchy random projections. *IEEE Transactions on Signal Processing*, 60(11):5725–5737.
- Redmond, M. and Baveja, A. (2002). A data-driven software tool for enabling cooperative information sharing among police departments. *Eur. J. Oper. Res.*, 141:660–678.
- Reeve, H. W., Kabán, A., and Bootkrajang, J. (2024). Heterogeneous sets in dimensionality reduction and ensemble learning. *Machine Learning*, 113(4):1683–1704.
- Ruan, L. and Yuan, M. (2010). Dimension reduction and parameter estimation for additive index models. *Statistics and its Interface*, 3(4):493–499.
- Slawski, M. (2018). On principal components regression, random projections, and column subsampling. *Electron. J. Statist.*, 12:3673 – 3712.
- Thanei, G.-A., Heinze, C., and Meinshausen, N. (2017). Random projections for large-scale regression. *Big and Complex Data Analysis: Methodologies and Applications*, pages 51–68.
- Tibshirani, R. (1996). Regression shrinkage and selection via the lasso. *Journal of the Royal Statistical Society: Series B*, 58(1):267–288.
- Tropp, J. A. (2012). User-friendly tail bounds for sums of random matrices. *Foundations of Computational Mathematics*, 12:389–434.
- Vershynin, R. (2018). *High-Dimensional Probability: An Introduction with Applications in Data Science*. Cambridge Series in Statistical and Probabilistic Mathematics. Cambridge University Press.
- Wainwright, M. J. (2019). *High-dimensional statistics: A non-asymptotic viewpoint*, volume 1. Cambridge University Press.
- Wang, T., Dobriban, E., Gataric, M., and Samworth, R. J. (2024). Sharp-SSL: Selective high-dimensional axis-aligned random projections for semi-supervised learning. *Journal of the American Statistical Association*, pages 1–13.
- Weisberg, S. (2002). Dimension reduction regression in R. *Journal of Statistical Software*, 7(1):1–22.

- Xia, Y., Tong, H., Li, W. K., and Zhu, L.-X. (2002). An adaptive estimation of dimension reduction space. *Journal of the Royal Statistical Society. Series B (Statistical Methodology)*, 64(3):363–410.
- Xie, H., Li, J., and Xue, H. (2017). A survey of dimensionality reduction techniques based on random projection. *arXiv preprint arXiv:1706.04371*.
- Yang, D., Ma, Z., and Buja, A. (2014). A sparse singular value decomposition method for high-dimensional data. *Journal of Computational and Graphical Statistics*, 23(4):923–942.
- Yu, Y., Wang, T., and Samworth, R. J. (2015). A useful variant of the Davis–Kahan theorem for statisticians. *Biometrika*, 102(2):315–323.
- Zhang, J., Wu, R., and Chen, X. (2023). Sparse sliced inverse regression via random projection. *arXiv preprint arXiv:2305.05141*.
- Zhou, F., Claire, Q., and King, R. D. (2014). Predicting the geographical origin of music. *2014 IEEE International Conference on Data Mining*, pages 1115–1120.
- Zou, H. and Hastie, T. (2005). Regularization and variable selection via the elastic net. *Journal of the Royal Statistical Society, Series B*, 67(2):301–320.

A Technical results and proofs

The main aim of this section is to prove Theorem 1, for which we will make use of the following basic technical lemma, see, for example, [Horn and Johnson \(2012, Theorem 4.2.2\)](#).

Lemma 2. *Let $A \in \mathbb{R}^{p \times p}$ be symmetric matrix, let $\lambda_1, \dots, \lambda_p$ be the eigenvalues of A , $\lambda_{max} := \max(\lambda_1, \dots, \lambda_p)$, $\lambda_{min} := \min(\lambda_1, \dots, \lambda_p)$. Then $\lambda_{max} = \max_{\|v\|_2=1} v^T A v$, and $\lambda_{min} = \min_{\|v\|_2=1} v^T A v$.*

Proof of Theorem 1. Recall from Algorithm 1 that $\hat{\Pi} = \frac{1}{L} \sum_{\ell=1}^L \mathbf{P}_{\ell,*} \mathbf{P}_{\ell,*}^T$ and \hat{A}_0^L denotes the $\mathbb{R}^{p \times d_0}$ which has columns given by the eigenvectors of $\hat{\Pi}$ ordered according to the corresponding eigenvalues. Recall also that $\Pi^\infty = \mathbb{E} \mathbf{P}_{\ell,*} \mathbf{P}_{\ell,*}^T$. Let $\Pi := A_0 A_0^T \in \mathbb{R}^{p \times p}$, and for $j \in [d_0]$ write a_j for the j th column of A_0 , so that $A_0 = (a_1, \dots, a_{d_0})$. Since $A_0^T A_0 = I_{d_0 \times d_0}$, the d_0 largest eigenvalues of Π are 1 and the remainder are 0. Indeed, $\text{rank}(\Pi) = \text{rank}(A_0) = d_0$, so Π has d_0 nonzero eigenvalues. Moreover, $\Pi a_j = A_0 A_0^T a_j = A_0 (A_0^T a_j) = A_0 e_j = a_j$ for $j \in [d_0]$. Then, since Π and $\hat{\Pi}$ are symmetric, by the Davis–Kahan Theorem ([Yu et al., 2015, Theorem 2](#)) we have

$$\begin{aligned} d_F(\mathcal{S}(\hat{A}_0^L), \mathcal{S}(A_0)) &\equiv \|\sin \Theta(\hat{A}_0^L, A_0)\|_F \leq 2d_0^{1/2} \|\hat{\Pi} - \Pi\|_{\text{op}} \\ &\leq 2d_0^{1/2} \left(\|\hat{\Pi} - \Pi^\infty\|_{\text{op}} + \|\Pi^\infty - \Pi\|_{\text{op}} \right). \end{aligned} \tag{6}$$

The second term in (6) doesn't depend on L nor the randomness in the projections. The remainder of the proof therefore involves controlling the expectation of the first term in (6). To that end, we first show that

$$\mathbb{P}\left(\|\hat{\Pi} - \Pi^\infty\|_{\text{op}} \geq t\right) \leq p \cdot e^{-t^2 L/8} \quad (7)$$

for $t > 0$. To see this, for $\ell \in [L]$ let $\Pi_\ell := \mathbf{P}_{\ell,*} \mathbf{P}_{\ell,*}^T$ and write $J_\ell := \frac{1}{L}(\Pi_\ell - \Pi^\infty)$, then

$$\hat{\Pi} - \Pi^\infty = \frac{1}{L} \sum_{\ell=1}^L \mathbf{P}_{\ell,*} \mathbf{P}_{\ell,*}^T - \Pi^\infty = \sum_{\ell=1}^L J_\ell.$$

Further $\mathbb{E}(J_\ell) = 0$ and J_ℓ (and thus also J_ℓ^2) is symmetric. Now, we show that $J_\ell^2 \preceq \frac{1}{L^2} I_{p \times p}$, in other words $\frac{1}{L^2} I_{p \times p} - J_\ell^2$ is positive semidefinite, almost surely, or equivalently that

$$\sup_{\{v: \|v\|=1\}} v^T J_\ell^2 v \leq \frac{1}{L^2}. \quad (8)$$

First, since $\mathbf{P}_{\ell,*}^T \mathbf{P}_{\ell,*} = I_{d \times d}$, the eigenvalues of Π_ℓ take values in $\{0, 1\}$ and we have by Lemma 2 that $0 \leq v^T \Pi_\ell v \leq 1$ whenever $\|v\|_2 = 1$. Moreover, by the linearity of expectation, we also have

$$v^T \Pi^\infty v = v^T \mathbb{E}(\Pi_\ell) v = \mathbb{E}(v^T \Pi_\ell v) \in [0, 1]$$

whenever $\|v\|_2 = 1$. It follows that

$$v^T (\Pi_\ell - \Pi^\infty) v = v^T \Pi_\ell v - v^T \Pi^\infty v \in [-1, 1], \quad \text{for all } \|v\|_2 = 1.$$

Hence we can write $\Pi_\ell - \Pi^\infty = U_\ell D_\ell U_\ell^T$, where $U_\ell \in \mathbb{R}^{p \times p}$ is orthonormal and D_ℓ is a diagonal $p \times p$ matrix with all entries between -1 and 1 (Horn and Johnson, 2012, Corollary 2.5.11). We deduce that, for all $v \in \mathbb{R}^p$ with $\|v\|_2 = 1$, we have

$$v^T J_\ell^2 v = \frac{1}{L^2} v^T (\Pi_\ell - \Pi^\infty)^2 v = \frac{1}{L^2} v^T U_\ell D_\ell^2 U_\ell^T v \leq \frac{1}{L^2} \|U_\ell^T v\| = \frac{1}{L^2},$$

which establishes (8).

Finally, because each of the projections $\mathbf{P}_{\ell,*}$ is chosen from a disjoint group of independently generated random projections, we have that $\mathbf{P}_{\ell,*}$ for $\ell \in [L]$ are independent and therefore J_ℓ for $\ell \in [L]$ are also independent. It then follows by the Matrix Hoeffding inequality (see, for example Tropp (2012, Theorem 1.3)), that

$$\mathbb{P}\left(\|\hat{\Pi} - \Pi^\infty\|_{\text{op}} \geq t\right) \leq p \cdot e^{-\frac{t^2}{8 \|\sum_{\ell=1}^L \frac{I_{p \times p}}{L^2}\|_{\text{op}}}} = p \cdot e^{-\frac{t^2 L}{8}},$$

which establishes the bound in (7). To complete the proof we bound the expectation as follows:

$$\begin{aligned} \mathbb{E}\left(\|\hat{\Pi} - \Pi^\infty\|_{\text{op}}\right) &= \int_0^\infty \mathbb{P}\left(\|\hat{\Pi} - \Pi^\infty\|_{\text{op}} \geq t\right) dt \\ &\leq \int_0^\infty p \cdot e^{-\frac{t^2 L}{8}} dt = \frac{p\sqrt{2\pi}}{\sqrt{L}}, \end{aligned}$$

as required. \square

B Full simulation results

In this section, we present the full results of our simulation study, which follows the design of the experiments described in Section 5 in the main text. Here, for each model, we consider the settings with $p \in \{20, 50, 100\}$ and $n \in \{50, 200, 500\}$. The full description of the algorithms considered, along with how any tuning parameters were chosen, is given in Section 5. To save space, rather than presenting boxplots here, we instead focus on the mean and standard error of the the sin-theta distance (when d_0 is known) over 100 repeats of the experiments. The results are given in Table 2 (for Models 1a-4) and Table 3 (for Models 5-9).

Setting		Competing Methods						Our Methods			
Model	p	n	SIR	pHd	MAVE	DR	gKDR	drMARS	RPE	RPE2	
1a ($d_0 = 1$)	20	50	0.97 _{0.05}	0.81 _{0.10}	0.87 _{0.14}	0.97 _{0.05}	0.92 _{0.09}	0.13 _{0.18}	0.32 _{0.14}	0.12_{0.04}	
		200	0.97 _{0.05}	0.40 _{0.08}	0.24 _{0.04}	0.33 _{0.06}	0.29 _{0.06}	0.03_{0.01}	0.20 _{0.11}	0.06 _{0.02}	
		500	0.96 _{0.07}	0.24 _{0.05}	0.10 _{0.02}	0.19 _{0.03}	0.14 _{0.03}	0.01_{0.01}	0.13 _{0.08}	0.05 _{0.02}	
	50	50	/	/	0.93 _{0.09}	/	0.97 _{0.03}	0.34 _{0.28}	0.46 _{0.17}	0.14_{0.08}	
		200	0.99 _{0.02}	0.74 _{0.09}	0.93 _{0.08}	0.65 _{0.12}	0.98 _{0.04}	0.04_{0.01}	0.32 _{0.17}	0.06 _{0.02}	
		500	0.98 _{0.04}	0.43 _{0.06}	0.42 _{0.12}	0.34 _{0.04}	0.57 _{0.20}	0.02_{0.02}	0.28 _{0.15}	0.05 _{0.02}	
	100	50	/	/	0.95 _{0.07}	/	0.98 _{0.02}	0.33 _{0.28}	0.57 _{0.17}	0.29_{0.29}	
		200	1.00 _{0.00}	0.95 _{0.03}	0.97 _{0.04}	0.99 _{0.01}	0.99 _{0.02}	0.05_{0.02}	0.46 _{0.17}	0.06_{0.02}	
		500	0.99 _{0.01}	0.72 _{0.07}	0.94 _{0.08}	0.54 _{0.04}	0.99 _{0.02}	0.01_{0.01}	0.38 _{0.16}	0.05 _{0.02}	
	2 ($d_0 = 1$)	20	50	0.98 _{0.03}	0.97 _{0.03}	0.97 _{0.04}	0.97 _{0.05}	0.97 _{0.03}	0.95_{0.17}	0.97 _{0.08}	0.97 _{0.06}
			200	0.98 _{0.03}	0.98 _{0.03}	0.98 _{0.02}	0.97 _{0.03}	0.98 _{0.03}	0.56 _{0.46}	0.06_{0.05}	0.10 _{0.16}
			500	0.98 _{0.03}	0.97 _{0.04}	0.97 _{0.03}	0.97 _{0.05}	0.98 _{0.03}	0.18 _{0.32}	0.03_{0.00}	0.03_{0.00}
50		50	/	/	0.98 _{0.04}	/	0.99 _{0.01}	0.99 _{0.01}	0.96_{0.13}	0.98 _{0.05}	
		200	0.99 _{0.02}	0.99 _{0.01}	0.99 _{0.02}	0.99 _{0.02}	0.99 _{0.01}	0.93 _{0.23}	0.09_{0.14}	0.27 _{0.37}	
		500	0.99 _{0.01}	0.99 _{0.02}	0.99 _{0.01}	0.99 _{0.01}	0.99 _{0.01}	0.60 _{0.47}	0.03_{0.01}	0.03_{0.01}	
100		50	/	/	0.99 _{0.02}	/	1.00 _{0.01}	0.98_{0.08}	1.00 _{0.01}	1.00 _{0.01}	
		200	0.99 _{0.04}	0.99 _{0.01}	0.99 _{0.02}	1.00 _{0.01}	1.00 _{0.01}	0.94 _{0.21}	0.16_{0.26}	0.40 _{0.42}	
		500	1.00 _{0.01}	0.99 _{0.01}	0.99 _{0.01}	1.00 _{0.01}	0.99 _{0.01}	0.77 _{0.41}	0.02_{0.01}	0.03 _{0.01}	
3 ($d_0 = 2$)		20	50	1.30 _{0.07}	1.27 _{0.08}	1.07 _{0.10}	1.29 _{0.07}	1.16 _{0.11}	0.92 _{0.28}	0.50_{0.31}	0.50_{0.30}
			200	0.85 _{0.13}	0.88 _{0.12}	0.72 _{0.13}	0.99 _{0.11}	0.89 _{0.12}	0.48 _{0.33}	0.10_{0.02}	0.10_{0.02}
			500	0.51 _{0.08}	0.55 _{0.08}	0.39 _{0.07}	0.67 _{0.11}	0.60 _{0.11}	0.27 _{0.26}	0.07_{0.01}	0.07_{0.01}
	50	50	/	/	1.12 _{0.10}	/	1.32 _{0.05}	1.21 _{0.17}	0.66_{0.34}	0.70_{0.33}	
		200	1.27 _{0.06}	1.29 _{0.06}	1.07 _{0.08}	1.23 _{0.07}	1.03 _{0.08}	0.54 _{0.27}	0.10_{0.03}	0.10_{0.04}	
		500	0.87 _{0.10}	0.93 _{0.09}	0.80 _{0.10}	0.98 _{0.09}	0.79 _{0.07}	0.32 _{0.25}	0.06_{0.01}	0.06_{0.01}	
	100	50	/	/	1.16 _{0.11}	/	1.37 _{0.02}	1.18 _{0.19}	0.71_{0.35}	0.80 _{0.31}	
		200	1.38 _{0.05}	1.38 _{0.02}	1.09 _{0.08}	1.29 _{0.04}	1.22 _{0.04}	0.63 _{0.25}	0.10_{0.05}	0.11_{0.05}	
		500	1.22 _{0.05}	1.27 _{0.06}	1.06 _{0.06}	1.16 _{0.06}	0.94 _{0.05}	0.36 _{0.27}	0.06_{0.01}	0.07 _{0.01}	
	4 ($d_0 = 1$)	20	50	0.90 _{0.10}	0.93 _{0.08}	0.51_{0.12}	0.85 _{0.13}	0.65 _{0.13}	0.50_{0.21}	0.53 _{0.12}	0.48_{0.19}
			200	0.30 _{0.06}	0.61 _{0.11}	0.29 _{0.05}	0.37 _{0.07}	0.38 _{0.08}	0.28 _{0.22}	0.34 _{0.14}	0.16_{0.04}
			500	0.17 _{0.03}	0.38 _{0.08}	0.18 _{0.03}	0.23 _{0.04}	0.23 _{0.04}	0.14 _{0.13}	0.29 _{0.12}	0.11_{0.03}
50		50	/	/	0.55_{0.15}	/	0.86 _{0.09}	0.82 _{0.20}	0.66 _{0.12}	0.55_{0.19}	
		200	0.67 _{0.12}	0.90 _{0.08}	0.43 _{0.06}	0.60 _{0.07}	0.49 _{0.06}	0.32 _{0.10}	0.61 _{0.15}	0.14_{0.04}	
		500	0.30 _{0.03}	0.66 _{0.09}	0.30 _{0.03}	0.37 _{0.04}	0.34 _{0.04}	0.18 _{0.09}	0.53 _{0.15}	0.09_{0.03}	
100		50	/	/	0.61_{0.16}	/	0.95 _{0.04}	0.82 _{0.20}	0.74 _{0.10}	0.62_{0.18}	
		200	0.99 _{0.01}	0.98 _{0.02}	0.46 _{0.06}	0.77 _{0.07}	0.64 _{0.06}	0.41 _{0.09}	0.70 _{0.10}	0.14_{0.04}	
		500	0.52 _{0.05}	0.88 _{0.06}	0.39 _{0.04}	0.52 _{0.04}	0.41 _{0.03}	0.20 _{0.10}	0.63 _{0.15}	0.09_{0.03}	

Table 2: The average sin-theta distance between \hat{A}_0 and A_0 over 100 repeats of the experiment for Models 1a, 2, 3 and 4, with $p \in \{20, 50, 100\}$ and $n \in \{50, 200, 500\}$. We compare two versions of our method with seven competing existing approaches. For each setting, we also present 10 times the standard error for each method in subscript. The “/” entries denote the the method is not applicable.

Setting			Competing Methods					Our Methods		
Model	p	n	SIR	pHd	MAVE	DR	gKDR	drMARS	RPE	RPE2
5 ($d_0 = 2$)	20	50	1.28 _{0.07}	1.33 _{0.06}	1.15 _{0.09}	1.25 _{0.09}	1.15 _{0.08}	1.06 _{0.19}	1.06 _{0.09}	1.03_{0.13}
		200	1.00 _{0.06}	1.07 _{0.08}	0.95 _{0.12}	1.01 _{0.08}	0.95 _{0.09}	0.73_{0.31}	1.00 _{0.00}	0.93 _{0.22}
		500	0.85 _{0.12}	0.99 _{0.05}	0.64 _{0.14}	0.85 _{0.12}	0.74 _{0.13}	0.44_{0.33}	1.00 _{0.00}	0.66 _{0.39}
	50	50	/	/	1.20 _{0.10}	/	1.30 _{0.05}	1.29 _{0.12}	1.12_{0.11}	1.13_{0.10}
		200	1.24 _{0.05}	1.38 _{0.03}	1.15 _{0.05}	1.18 _{0.05}	1.09 _{0.05}	0.84_{0.29}	1.00 _{0.00}	0.97 _{0.14}
		500	1.04 _{0.04}	1.11 _{0.07}	1.06 _{0.05}	1.05 _{0.04}	0.95 _{0.05}	0.50_{0.30}	1.00 _{0.00}	0.70 _{0.36}
	100	50	/	/	1.25 _{0.08}	/	1.36 _{0.03}	1.30 _{0.12}	1.15_{0.13}	1.19 _{0.11}
		200	1.40 _{0.02}	1.40 _{0.01}	1.18 _{0.04}	1.27 _{0.03}	1.20 _{0.04}	1.02 _{0.21}	1.00 _{0.00}	0.96_{0.15}
		500	1.17 _{0.03}	1.39 _{0.03}	1.15 _{0.03}	1.15 _{0.03}	1.05 _{0.04}	0.53_{0.29}	1.00 _{0.00}	0.74 _{0.34}
6 ($d_0 = 3$)	20	50	1.59 _{0.06}	1.50 _{0.08}	1.38 _{0.12}	1.59 _{0.07}	1.52 _{0.08}	1.16 _{0.46}	1.14_{0.27}	1.20 _{0.26}
		200	1.58 _{0.07}	1.39 _{0.09}	1.26 _{0.15}	1.38 _{0.10}	1.16 _{0.13}	0.66_{0.56}	0.73_{0.28}	0.73_{0.29}
		500	1.59 _{0.06}	1.36 _{0.09}	0.41 _{0.05}	0.98 _{0.13}	0.69 _{0.10}	0.49 _{0.56}	0.36_{0.12}	0.36_{0.13}
	50	50	/	/	1.47 _{0.11}	/	1.64 _{0.03}	1.53 _{0.16}	1.36_{0.23}	1.44 _{0.16}
		200	1.68 _{0.02}	1.59 _{0.04}	1.55 _{0.06}	1.65 _{0.03}	1.65 _{0.03}	1.09_{0.51}	1.08_{0.35}	1.18 _{0.36}
		500	1.67 _{0.03}	1.54 _{0.05}	1.53 _{0.06}	1.49 _{0.07}	1.47 _{0.06}	0.66_{0.65}	0.67_{0.31}	0.66_{0.32}
	100	50	/	/	1.54 _{0.11}	/	1.68 _{0.02}	1.50_{0.21}	1.51_{0.17}	1.56 _{0.14}
		200	1.71 _{0.03}	1.68 _{0.02}	1.56 _{0.05}	1.70 _{0.01}	1.69 _{0.02}	1.29_{0.46}	1.31_{0.23}	1.41 _{0.21}
		500	1.70 _{0.01}	1.64 _{0.02}	1.63 _{0.04}	1.67 _{0.03}	1.69 _{0.02}	0.88_{0.65}	1.02 _{0.34}	1.12 _{0.38}
7 ($d_0 = 2$)	20	50	1.34 _{0.05}	1.29 _{0.06}	1.23 _{0.11}	1.33 _{0.06}	1.30 _{0.08}	1.09_{0.24}	1.13 _{0.19}	1.15 _{0.18}
		200	1.34 _{0.05}	1.13 _{0.11}	1.05 _{0.15}	1.07 _{0.08}	1.02 _{0.07}	0.60_{0.23}	0.65 _{0.19}	0.61_{0.22}
		500	1.33 _{0.06}	0.99 _{0.13}	0.54 _{0.22}	0.95 _{0.09}	0.78 _{0.16}	0.55 _{0.16}	0.55_{0.02}	0.54_{0.17}
	50	50	/	/	1.30 _{0.09}	/	1.36 _{0.03}	1.28 _{0.16}	1.22_{0.18}	1.26 _{0.17}
		200	1.39 _{0.02}	1.31 _{0.05}	1.29 _{0.07}	1.33 _{0.06}	1.37 _{0.04}	0.67_{0.29}	0.79 _{0.22}	0.78 _{0.27}
		500	1.39 _{0.02}	1.21 _{0.09}	1.20 _{0.09}	1.10 _{0.05}	1.20 _{0.09}	0.56 _{0.20}	0.57 _{0.01}	0.53_{0.11}
	100	50	/	/	1.35 _{0.07}	/	1.39 _{0.02}	1.25_{0.17}	1.31 _{0.13}	1.33 _{0.11}
		200	1.40 _{0.01}	1.39 _{0.02}	1.32 _{0.06}	1.40 _{0.01}	1.39 _{0.02}	0.87_{0.31}	0.95 _{0.26}	1.01 _{0.26}
		500	1.40 _{0.01}	1.33 _{0.04}	1.33 _{0.06}	1.30 _{0.06}	1.39 _{0.02}	0.53_{0.17}	0.58 _{0.01}	0.56 _{0.08}
8 ($d_0 = 2$)	20	50	1.30 _{0.08}	1.21 _{0.07}	1.02 _{0.11}	1.29 _{0.07}	1.16 _{0.13}	0.38 _{0.30}	0.21_{0.15}	0.20_{0.12}
		200	1.03 _{0.15}	1.03 _{0.07}	0.71 _{0.12}	0.92 _{0.13}	0.83 _{0.13}	0.20 _{0.13}	0.08_{0.02}	0.08_{0.02}
		500	0.68 _{0.13}	0.88 _{0.19}	0.38 _{0.07}	0.68 _{0.14}	0.58 _{0.12}	0.07 _{0.05}	0.07_{0.01}	0.07_{0.01}
	50	50	/	/	1.11 _{0.11}	/	1.32 _{0.05}	0.73 _{0.30}	0.24_{0.24}	0.27 _{0.24}
		200	1.34 _{0.05}	1.20 _{0.04}	1.02 _{0.06}	1.16 _{0.06}	1.13 _{0.09}	0.26 _{0.16}	0.08_{0.01}	0.08_{0.01}
		500	1.06 _{0.11}	1.07 _{0.02}	0.82 _{0.08}	0.94 _{0.10}	0.83 _{0.08}	0.14 _{0.10}	0.07_{0.01}	0.07_{0.01}
	100	50	/	/	1.15 _{0.10}	/	1.37 _{0.02}	0.81 _{0.27}	0.33_{0.31}	0.35_{0.29}
		200	1.40 _{0.01}	1.36 _{0.02}	1.06 _{0.06}	1.32 _{0.04}	1.28 _{0.05}	0.36 _{0.14}	0.07_{0.01}	0.08 _{0.02}
		500	1.34 _{0.04}	1.19 _{0.04}	0.99 _{0.05}	1.10 _{0.05}	1.06 _{0.07}	0.17 _{0.12}	0.07_{0.01}	0.07_{0.01}
9 ($d_0 = 2$)	20	50	1.30 _{0.07}	1.31 _{0.06}	1.21 _{0.09}	1.32 _{0.07}	1.22 _{0.07}	0.95_{0.32}	1.00 _{0.15}	1.02 _{0.16}
		200	1.06 _{0.05}	1.17 _{0.08}	1.12 _{0.06}	1.18 _{0.09}	1.17 _{0.07}	0.31 _{0.43}	0.18_{0.21}	0.18_{0.22}
		500	1.00 _{0.04}	1.08 _{0.05}	1.03 _{0.04}	1.06 _{0.04}	1.08 _{0.05}	0.14 _{0.31}	0.07_{0.02}	0.07_{0.02}
	50	50	/	/	1.25 _{0.08}	/	1.33 _{0.04}	1.24 _{0.15}	1.07_{0.16}	1.12 _{0.17}
		200	1.30 _{0.06}	1.33 _{0.04}	1.22 _{0.04}	1.30 _{0.05}	1.18 _{0.04}	0.69 _{0.43}	0.27_{0.30}	0.28_{0.30}
		500	1.09 _{0.03}	1.21 _{0.05}	1.15 _{0.03}	1.18 _{0.06}	1.15 _{0.04}	0.47 _{0.48}	0.09_{0.06}	0.09_{0.06}
	100	50	/	/	1.28 _{0.07}	/	1.37 _{0.02}	1.24 _{0.16}	1.07_{0.18}	1.13 _{0.15}
		200	1.40 _{0.03}	1.39 _{0.02}	1.23 _{0.05}	1.34 _{0.03}	1.27 _{0.04}	0.89 _{0.36}	0.35_{0.35}	0.37_{0.36}
		500	1.26 _{0.05}	1.33 _{0.04}	1.22 _{0.03}	1.26 _{0.04}	1.15 _{0.02}	0.53 _{0.48}	0.11_{0.18}	0.11_{0.18}

Table 3: The average sin-theta distance between \hat{A}_0 and A_0 over 100 repeats of the experiment for Models 5-9, with $p \in \{20, 50, 100\}$ and $n \in \{50, 200, 500\}$. We compare two versions of our method with seven competing existing approaches. For each setting, we also present 10 times the standard error for each method in subscript. The “/” entries denote the the method is not applicable.

The broad message from the results in Tables 2 and 3 is that our random projection based algorithms are competitive across the 9 models, for different values of n and p . Indeed, the relative performance is somewhat similar to the $p = 50$ and $n = 200$ case presented in the main text. There are some additional points worth noting here. First, when $n = 50$ and $p \in \{50, 100\}$ so that $p \geq n$, the SIR, pHd and DR methods are not

applicable. Overall, our approach enjoys the best performance for Models 2, 3, 4, 8 and 9. For the remaining models, the performance of our random projection based method and drMARS is close, and these outperform the other competitors.

B.1 Computational cost

In this section we investigate the actual runtime in seconds of the different methods we consider. In Table 4, we present the run time for one run of the experiment for Model 1a, for different values of n and p . The second right column, with label ‘RPE’, shows the running time of the experiment on a single core of a 3.20 GHz Intel i9-14900KF computer. We also demonstrate the potential speed up that may be gained using parallel computing – the RPE (10 cores) column presents the runtime of algorithm using ten cores of a 3.20 GHz Intel i9-14900KF computer. Using parallel computing in this example results in approximately seven times faster compute time.

Setting		Competing Methods						Our Methods	
p	n	SIR	pHd	MAVE	DR	gKDR	drMARS	RPE	RPE(10 cores)
	50	0.007	0.007	0.051	0.009	0.015	0.138	120.151	18.043
20	200	0.007	0.005	0.408	0.007	0.078	0.211	146.465	22.750
	500	0.008	0.006	0.961	0.008	0.381	0.276	194.996	28.899
	50	/	/	0.047	/	0.026	0.185	367.642	56.797
50	200	0.011	0.007	0.827	0.013	0.224	0.478	508.912	73.372
	500	0.014	0.009	2.988	0.020	1.006	0.635	697.639	98.825
	50	/	/	0.047	/	0.109	0.188	1302.905	276.516
100	200	0.032	0.016	0.820	0.018	0.778	0.841	1724.973	300.544
	500	0.033	0.020	7.945	0.031	3.327	1.162	2040.819	356.924

Table 4: The runtime in seconds of the methods considered for the simulations for Model 1a, with $p \in \{20, 50, 100\}$ and $n \in \{50, 200, 500\}$. The “/” entries denote the the method is not applicable.

B.2 Dimension d_0 unknown

Tables 5 and 6 show the full results for the false positive and false negative metrics of additional experiments corresponding to those in Section 5.2. We present the results for $p \in \{20, 50, 100\}$ and $n = 200$. Results for $n = 50$ and $n = 500$, which are broadly similar, are omitted for brevity.

Setting		Competing Methods					Our Methods
Model	p	SIR	pHd	MAVE	gKDR	drMARS	RPE
1a ($d_0 = 1$)	20	0.06 _{0.23}	0.07 _{0.17}	0.24 _{0.04}	1.48 _{0.60}	1.15 _{0.76}	1.00 _{0.00}
	50	0.04 _{0.20}	0.00 _{0.00}	0.93 _{0.08}	2.22 _{0.33}	1.54 _{0.80}	1.00 _{0.04}
	100	0.00 _{0.00}	0.00 _{0.00}	0.97 _{0.04}	2.87 _{0.26}	1.82 _{0.84}	1.07 _{0.21}
2 ($d_0 = 1$)	20	0.04 _{0.22}	0.00 _{0.00}	1.68 _{0.20}	1.51 _{0.42}	1.33 _{0.58}	0.59 _{0.59}
	50	0.02 _{0.14}	0.00 _{0.00}	1.70 _{0.12}	2.13 _{0.47}	1.81 _{0.62}	1.02 _{0.83}
	100	0.00 _{0.00}	0.00 _{0.00}	1.68 _{0.13}	2.63 _{0.38}	1.90 _{0.70}	1.65 _{1.07}
3 ($d_0 = 2$)	20	0.46 _{0.25}	0.04 _{0.15}	0.92 _{0.30}	1.23 _{0.52}	1.06 _{0.63}	0.10 _{0.02}
	50	0.19 _{0.40}	0.00 _{0.00}	1.34 _{0.21}	1.94 _{0.46}	1.50 _{0.73}	0.19 _{0.29}
	100	0.00 _{0.00}	0.00 _{0.00}	1.35 _{0.20}	2.55 _{0.41}	1.54 _{0.84}	0.35 _{0.47}
4 ($d_0 = 1$)	20	0.32 _{0.19}	0.00 _{0.00}	1.06 _{0.35}	1.32 _{0.61}	1.09 _{0.67}	1.42 _{0.00}
	50	0.09 _{0.25}	0.00 _{0.00}	1.27 _{0.21}	2.10 _{0.49}	1.50 _{0.81}	1.44 _{0.09}
	100	0.00 _{0.00}	0.00 _{0.00}	1.28 _{0.20}	2.49 _{0.45}	1.72 _{0.83}	1.54 _{0.18}
5 ($d_0 = 2$)	20	0.35 _{0.21}	0.01 _{0.10}	0.98 _{0.34}	1.45 _{0.47}	0.97 _{0.55}	1.01 _{0.01}
	50	0.09 _{0.28}	0.00 _{0.00}	1.40 _{0.19}	2.06 _{0.39}	1.47 _{0.67}	1.05 _{0.13}
	100	0.00 _{0.00}	0.00 _{0.00}	1.41 _{0.18}	2.52 _{0.40}	1.55 _{0.72}	1.19 _{0.25}
6 ($d_0 = 3$)	20	0.03 _{0.15}	0.00 _{0.00}	1.26 _{0.29}	0.85 _{0.37}	0.59 _{0.57}	1.01 _{0.46}
	50	0.00 _{0.00}	0.00 _{0.00}	1.55 _{0.23}	1.47 _{0.56}	1.10 _{0.79}	1.97 _{0.56}
	100	0.00 _{0.00}	0.00 _{0.00}	1.56 _{0.22}	2.55 _{0.50}	1.36 _{0.73}	2.47 _{0.62}
7 ($d_0 = 2$)	20	0.02 _{0.13}	0.00 _{0.00}	1.31 _{0.32}	1.00 _{0.53}	0.87 _{0.57}	0.99 _{0.44}
	50	0.02 _{0.13}	0.00 _{0.00}	1.61 _{0.17}	1.91 _{0.55}	1.23 _{0.77}	1.63 _{0.65}
	100	0.00 _{0.00}	0.00 _{0.00}	1.63 _{0.16}	2.56 _{0.41}	1.52 _{0.82}	2.26 _{0.79}
8 ($d_0 = 2$)	20	0.37 _{0.34}	0.11 _{0.17}	0.48 _{0.24}	1.56 _{0.40}	0.99 _{0.63}	0.08 _{0.02}
	50	0.12 _{0.35}	0.00 _{0.00}	0.82 _{0.25}	2.23 _{0.35}	1.42 _{0.71}	0.09 _{0.09}
	100	0.00 _{0.00}	0.00 _{0.00}	0.90 _{0.22}	2.65 _{0.35}	1.62 _{0.80}	0.18 _{0.31}
9 ($d_0 = 2$)	20	0.29 _{0.28}	0.00 _{0.00}	1.45 _{0.24}	1.63 _{0.40}	0.86 _{0.64}	0.11 _{0.14}
	50	0.10 _{0.29}	0.00 _{0.00}	1.53 _{0.16}	2.23 _{0.38}	1.26 _{0.80}	0.28 _{0.36}
	100	0.00 _{0.00}	0.00 _{0.00}	1.52 _{0.16}	2.67 _{0.39}	1.74 _{0.81}	0.41 _{0.51}

Table 5: The average of $d_{\text{FP}}(\mathcal{S}(\hat{A}_0), \mathcal{S}(A_0))$ over 100 repeats of the experiment for Models 1a-9, with $p \in \{20, 50, 100\}$ and $n = 200$. For each setting, we also present 10 times the standard error for each method in subscript.

Setting		Competing Methods					Our Methods
Model	p	SIR	pHd	MAVE	gKDR	drMARS	RPE
1a ($d_0 = 1$)	20	0.99 _{0.04}	0.88 _{0.25}	0.24 _{0.04}	0.25 _{0.06}	0.02 _{0.02}	0.05 _{0.01}
	50	1.00 _{0.00}	1.00 _{0.00}	0.93 _{0.08}	0.69 _{0.15}	0.02 _{0.01}	0.04 _{0.01}
	100	1.00 _{0.00}	1.00 _{0.00}	0.97 _{0.04}	0.83 _{0.07}	0.03 _{0.02}	0.04 _{0.00}
2 ($d_0 = 1$)	20	1.00 _{0.00}	1.00 _{0.00}	0.92 _{0.07}	0.94 _{0.05}	0.48 _{0.46}	0.05 _{0.02}
	50	1.00 _{0.00}	1.00 _{0.00}	0.96 _{0.03}	0.95 _{0.04}	0.87 _{0.29}	0.07 _{0.04}
	100	1.00 _{0.00}	1.00 _{0.00}	0.97 _{0.03}	0.96 _{0.02}	0.90 _{0.25}	0.09 _{0.08}
3 ($d_0 = 2$)	20	1.07 _{0.16}	1.40 _{0.07}	0.69 _{0.12}	0.88 _{0.17}	0.43 _{0.34}	0.10 _{0.02}
	50	1.40 _{0.05}	1.41 _{0.00}	1.02 _{0.09}	0.96 _{0.08}	0.48 _{0.28}	0.10 _{0.03}
	100	1.41 _{0.00}	1.41 _{0.00}	1.05 _{0.09}	1.12 _{0.06}	0.56 _{0.30}	0.10 _{0.09}
4 ($d_0 = 1$)	20	0.35 _{0.19}	1.00 _{0.00}	0.27 _{0.05}	0.35 _{0.07}	0.18 _{0.08}	0.11 _{0.03}
	50	0.96 _{0.11}	1.00 _{0.00}	0.40 _{0.05}	0.44 _{0.05}	0.26 _{0.10}	0.09 _{0.02}
	100	1.00 _{0.00}	1.00 _{0.00}	0.43 _{0.06}	0.58 _{0.05}	0.32 _{0.12}	0.09 _{0.02}
5 ($d_0 = 2$)	20	1.11 _{0.13}	1.41 _{0.00}	0.94 _{0.14}	0.88 _{0.14}	0.55 _{0.40}	0.93 _{0.23}
	50	1.41 _{0.04}	1.41 _{0.00}	1.13 _{0.06}	1.02 _{0.06}	0.61 _{0.34}	0.97 _{0.16}
	100	1.41 _{0.00}	1.41 _{0.00}	1.16 _{0.05}	1.15 _{0.04}	0.89 _{0.31}	0.95 _{0.17}
6 ($d_0 = 3$)	20	1.73 _{0.02}	1.73 _{0.00}	1.26 _{0.17}	1.37 _{0.22}	1.04 _{0.56}	0.63 _{0.25}
	50	1.71 _{0.00}	1.73 _{0.00}	1.55 _{0.07}	1.63 _{0.11}	1.22 _{0.48}	0.93 _{0.35}
	100	1.73 _{0.00}	1.73 _{0.00}	1.57 _{0.07}	1.63 _{0.05}	1.28 _{0.50}	1.15 _{0.28}
7 ($d_0 = 2$)	20	1.41 _{0.00}	1.41 _{0.00}	0.98 _{0.15}	1.01 _{0.11}	0.61 _{0.39}	0.56 _{0.20}
	50	1.41 _{0.01}	1.41 _{0.00}	1.23 _{0.06}	1.27 _{0.11}	0.61 _{0.40}	0.62 _{0.23}
	100	1.41 _{0.00}	1.41 _{0.00}	1.28 _{0.08}	1.32 _{0.05}	0.81 _{0.37}	0.80 _{0.26}
8 ($d_0 = 2$)	20	1.25 _{0.16}	1.31 _{0.16}	0.84 _{0.19}	0.73 _{0.14}	0.18 _{0.18}	0.08 _{0.02}
	50	1.41 _{0.02}	1.41 _{0.00}	1.07 _{0.09}	0.96 _{0.10}	0.19 _{0.11}	0.08 _{0.01}
	100	1.41 _{0.00}	1.41 _{0.00}	1.11 _{0.09}	1.15 _{0.06}	0.25 _{0.10}	0.07 _{0.01}
9 ($d_0 = 2$)	20	1.24 _{0.15}	1.41 _{0.08}	1.08 _{0.07}	1.11 _{0.10}	0.31 _{0.44}	0.26 _{0.34}
	50	1.40 _{0.04}	1.41 _{0.00}	1.20 _{0.05}	1.13 _{0.04}	0.68 _{0.44}	0.29 _{0.33}
	100	1.41 _{0.00}	1.41 _{0.00}	1.21 _{0.05}	1.22 _{0.04}	0.85 _{0.37}	0.34 _{0.36}

Table 6: The average of $d_{\text{FN}}(\mathcal{S}(\hat{A}_0), \mathcal{S}(A_0))$ over 100 repeats of the experiment for Models 1a-9, with $p \in \{20, 50, 100\}$ and $n = 200$. For each setting, we also present 10 times the standard error for each method in subscript.